FLAIRR-seq: A novel method for single molecule resolution of near full-length immunoglobulin heavy chain repertoires

Authors:

Easton E. Ford[1,2], David Tieri[2], Oscar Rodriguez[2], Nancy Francoeur[3], Juan Soto[3], Justin Kos[2], Ayelet Peres[4,5], William Gibson[2], Catherine A. Silver[2], Gintaras Deikus[3], Elizabeth Hudson[2], Cassandra R. Woolley[1], Noam Beckmann[3], Alexander Charney[3], Thomas C. Mitchell[1], Gur Yaari[4,5], Robert P. Sebra[3], Corey T. Watson[2*], Melissa L. Smith[2*]

Affiliations:

* denotes equal author contribution to the manuscript

[1]Department of Microbiology and Immunology University of Louisville School of Medicine, Louisville, Kentucky, USA

[2]Department of Biochemistry and Molecular Genetics University of Louisville School of Medicine, Louisville, Kentucky, USA

[3]Department of Genetics and Genomic Sciences, Icahn School of Medicine at Mount Sinai, New York City, New York, USA

[4] Faculty of Engineering, Bar Ilan University, 5290002 Ramat Gan, Israel

[5] Bar Ilan Institute of Nanotechnology and Advanced Materials, Bar Ilan University, 5290002, Ramat Gan, Israel

Corresponding Author:

Melissa L. Smith, PhD

ml.smith@louisville.edu

Abstract:

Current Adaptive Immune Receptor Repertoire Sequencing (AIRR-seq) strategies resolve expressed antibody (Ab) transcripts with limited resolution of the constant region. Here we present a novel near full-length AIRR-seq (FLAIRR-Seq) method that utilizes targeted amplification by 5' rapid amplification of cDNA ends (RACE), combined with single molecule, real-time sequencing to generate highly accurate (>Q40, 99.99%) IG heavy chain transcripts. FLAIRR-seq was benchmarked by comparing IG heavy chain variable (IGHV), diversity (IGHD), and joining (IGHJ) gene usage, complementarity-determining region 3 (CDR3) length, and somatic hypermutation to matched datasets generated with standard 5' RACE AIRR-seq and full-length isoform sequencing. Together these data demonstrate robust, unbiased FLAIRR-seq performance using RNA samples derived from peripheral blood mononuclear cells, purified B cells, and whole blood, which recapitulated results generated by commonly used methods, while additionally resolving novel IG heavy chain constant (IGHC) gene features. FLAIRR-seq data provides, for the first time, simultaneous, single-molecule characterization of IGHV, IGHD, IGHJ, and IGHC region genes and alleles, allele-resolved subisotype definition, and high-resolution identification of class-switch recombination within a clonal lineage. In conjunction with genomic sequencing and genotyping of IGHC genes, FLAIRR-seq of the IgM and IgG repertoires from 10 individuals resulted in the identification of 32 unique IGHC alleles, 28 (87%) of which were previously uncharacterized. Together, these data demonstrate the capabilities of FLAIRR-seq to characterize IGHV, IGHD, IGHJ, and IGHC gene diversity for the most comprehensive view of bulk expressed Ab repertoires to date.

52 **Introduction**

53 Antibodies (Abs) or immunoglobulins (IGs) are the primary effectors of humoral immunity
54 and are found as both membrane-bound receptors on B cells and circulating, secreted proteins
55 (1). Both membrane-bound B cell receptors (BCRs) and secreted Abs act to recognize and bind
56 antigen. All Abs and BCRs are composed of two identical heavy and light chains that are post-
57 translationally associated. The heavy chain is comprised of two distinct domains: (i) the variable
58 domain (Fab), which allows for antigen binding, and (ii) the constant domain (Fc), which
59 modulates downstream effector functions (1, 2). The light chain also includes a variable domain
60 that, once post-translationally associated with the heavy chain variable domain, interacts with
61 cognate antigen (3). In humans, Abs are grouped into discrete isotypes and subisotypes (i.e.,
62 IgM, IgD, IgG1, IgG2, IgG3, IgG4, IgA1, IgA2, and IgE), based on the expression of specific
63 constant (C) genes within the IG heavy chain locus (IGH). Each isotype and subisotype has
64 unique effector properties that together represent the wide diversity of Ab-mediated functions,
65 including binding of Fc receptors (FCR), activation of complement, opsonization, antibody-
66 dependent cellular cytotoxicity (ADCC) and antibody-dependent cellular phagocytosis (ADCP) (4,
67 5).

68 To facilitate the development of diverse Ab repertoires capable of recognizing the wide
69 range of pathogens humans encounter, the IG genomic loci are highly polymorphic and harbor
70 diverse and complex sets of genes that recombine in each B cell to encode up to 10^{13} unique
71 specificities (6). B cells create this expansive catalog of specificities through somatic
72 recombination of the variable (V), diversity (D), and joining (J) genes in IGH, and V and J genes
73 from the corresponding light chain loci, lambda (IGL) and kappa (IGK) (7). During VDJ
74 recombination in IGH, a single D and J gene are first recombined, while the intervening and
75 unselected D and J gene sequences are removed by RAG recombinase (8). After D and J genes
76 are joined, further recombination of a specific V gene to the DJ gene cassette completes the
77 formation of the full VDJ rearrangement. Following transcription of the recombined VDJ, a single

78 constant region gene is spliced together with the VDJ cassette to generate the completed heavy
79 chain transcript (7). Recombination at IGL and IGK occurs similarly, recombining V and J genes
80 only. Heavy and light chain transcripts are independently translated and linked via covalent
81 cysteine bonds resulting in a fully functional protein prior to B cell cell-surface expression or
82 secretion (Figure 1A) (9). Naïve B cells, which develop in the bone marrow from hematopoietic
83 stem cell progenitors, have undergone VDJ recombination but have not yet encountered antigen,
84 and solely express IgM and IgD (10). These naïve B cells then migrate to B cell zones in
85 secondary lymphoid tissues where they encounter antigen, driving further maturation and class
86 switch recombination (CSR) to enable the most effective humoral responses (11). CSR mediates
87 the excision of IGHC genes at the DNA level, which leads to the utilization and linkage of different
88 IGHC genes to the same VDJ, ultimately resulting in class switching to alternate isotypes and
89 subisotypes (11).

90 The IgG isotype class is represented by four subisotypes: IgG1, IgG2, IgG3, and IgG4.
91 Each IgG subisotype circulates at varied frequencies and facilitates unique immune functions. For
92 example, IgG1 is typically the most abundant circulating IgG and mediates proinflammatory
93 responses; IgG2 targets bacterial polysaccharides, providing protection from bacterial pathogens;
94 IgG3 confers protection against intracellular bacterial infections and enables clearing of parasites;
95 and IgG4 contains exclusive structural and functional characteristics often resulting in anti-
96 inflammatory and tolerance-inducing effects (5). Multiple studies have identified Ab-mediated
97 subisotype-specific pathogenicity in the context of autoimmune diseases and cancer highlighting
98 the need for further investigation of subisotype-specific repertoires (12-15).

99 Current Adaptive Immune Receptor Repertoire sequencing (AIRR-seq) methods aim to
100 resolve variable and constant region transcripts to differing extents. Profiling of the variable
101 region, even in part, defines V, D and J gene usage while also providing characterization of
102 complementarity determining regions (CDR) 1, 2, and 3, which are hypervariable and directly
103 interact with target antigen (Figure 1B) (16). CDR3-targeted profiling approaches, such as those

104 used by Adaptive Biotechnologies (17), allow for V, D, and J gene assignments but do not provide
105 complete resolution of the entire variable region (17). Multiplexed primer-based AIRR-seq
106 strategies generate full variable region content but require specific primers to known targets and
107 therefore may miss novel genes and alleles. 5' RACE AIRR-seq methods capture the full-length
108 VDJ exon without variable region-targeted multiplexed primer pools therefore limiting the impact
109 of primer bias and enabling discovery of novel IGHV, IGHD, and IGHJ genes and alleles (18). 5'
110 RACE methods also often prime from the first IGHC exon (CH1), allowing for determination of
111 isotype. Additional methods have been developed that shift amplification strategies by capturing
112 additional IGHC region sequence to enable subisotype resolution; however, these methods
113 sacrifice full and contiguous characterization of the IGHV gene (19). All commonly used AIRR-
114 seq methods are further technically limited by the length restrictions (≤ 600nt) of short-read next
115 generation sequencing. As a result, no current AIRR-seq strategy resolves the complete heavy
116 chain transcript, including all IGHC exons alongside the recombined IGHV, IGHD, and IGHJ
117 genes. Our team has recently shown that population-based polymorphisms within the IGHV,
118 IGHD, IGHJ and IGL loci are far more extensive than previously known; the IGHC region has also
119 been shown to contain genomic diversity, although the extent of this diversity has likely not been
120 fully explored (20-27). Although it is understood that the Fc domain mediates Ab effector
121 functions, there is limited knowledge as to how genetic variation in this region may impact
122 functional capabilities or posttranslational modification (5, 28, 29). As such, there is a growing
123 need to understand genomic variation across the complete Ab molecule. To address these
124 limitations, we have developed novel, end-to-end pipeline to target, profile, and characterize the
125 Ab heavy chain repertoire in the context of isotype (IgG, IgM) and subisotype (IgG1, IgG2, IgG3,
126 IgG4).

127 Here, we present FLAIRR-seq, a novel targeted 5' RACE-based amplification of near full-
128 length IgG and IgM heavy chain transcripts, paired with single molecule real time (SMRT)
129 sequencing, resulting in highly accurate (mean read accuracy ~Q60, 99.9999%), near full-length

130 Ab sequences from RNA derived from whole blood, isolated PBMC, and purified B cells. When
131 analyzed with the Immcantation AIRR-seq tool suite (30, 31), we demonstrate that FLAIRR-seq
132 performs comparably to standard 5'RACE AIRR-seq methods and single-molecule isoform
133 sequencing (Iso-Seq) strategies for characterizing the expressed Ab repertoire. We further
134 highlight the novel features of FLAIRR-seq data, including phased identification of IGHV, IGHD,
135 IGHJ, and IGHC genes, facilitating the profiling of subisotype- and IGHC allele-specific repertoires
136 and CSR characterization.
137

138 **Materials and Methods**

139 **Sample collections**

140 Experiments were conducted using healthy donor peripheral blood mononuclear cells
141 (PBMC), purified B cells from healthy donors, or whole blood collected from hospitalized COVID-
142 19 patients (Supplementary Table 1). Commercially available healthy donor PBMC (STEMCELL
143 Technologies) and a subset of matched purified B cells were utilized to generate AIRR-seq and
144 FLAIRR-seq validation datasets. Full-length isoform sequencing (Iso-Seq) was performed using
145 B cells isolated from the PBMC of a healthy, consented 57-year-old male donor at the University
146 of Louisville (UofL) School of Medicine. The UofL Institutional Review Board approved sample
147 collection (IRB 14.0661). For COVID-19 affected patient samples (n=5), whole blood was
148 collected from the Mount Sinai COVID-19 biobank cohort of hospitalized COVID-19 patients,
149 approved by the Institutional Review Board at the Icahn School of Medicine at Mount Sinai as
150 previously described (32).

151 **PBMC isolation and B cell purification**

152 Frozen healthy donor PBMCs were purchased, thawed, and aliquoted for use in
153 downstream experiments (STEMCELL Technologies). For Iso-Seq analyses, 175mL of venous
154 blood was collected in a final concentration of 6mM K_3EDTA using standard phlebotomy. PBMCs

155 were isolated using Sepmate PBMC Isolation Tubes (STEMCELL Technologies) as previously
156 described (33), with an additional granulocyte depletion step using the RosetteSep Human
157 Granulocyte Depletion Cocktail (STEMCELL Technologies) as directed by the manufacturer. B
158 cells from the freshly collected and frozen healthy donor PBMC were isolated using the EasySep
159 Human Pan-B Cell Enrichment Kit, as described by the manufacturer (STEMCELL Technologies).
160 Briefly, B cells, including plasma cells, were isolated by negative selection using coated magnetic
161 particles. First, the B cell enrichment cocktail was added to the sample and mixed for a 5-minute
162 incubation at room temperature, followed by addition of magnetic particles and further incubation
163 for 5 minutes on the benchtop. The sample tube was then placed on an EasySep magnet
164 (STEMCELL Technologies), and purified B cells were carefully eluted from the magnetic particles
165 and immediately used for RNA extraction.

166 **Genomic DNA and RNA extraction**

167 For the healthy frozen PBMC and matched purified B cells, genomic DNA (gDNA) and
168 RNA were co-extracted using the AllPrep DNA/RNA Mini Kit (Qiagen) according to the
169 manufacturer's instructions. For the freshly processed UofL healthy donor PBMC, purified Pan-B
170 cells were lysed in Buffer RLT Plus, and RNA was extracted with the RNeasy Plus Mini Kit
171 (Qiagen) per the manufacturer's protocol; no gDNA was collected from this sample. COVID-19
172 whole blood-derived RNA was extracted from samples collected in Tempus Blood RNA tubes
173 using the Tempus Spin RNA Isolation Kit (ThermoFisher) as described by the manufacturer. For
174 all samples, concentrations of RNA and gDNA (when appropriate) were assessed using the Qubit
175 4.0 fluorometer, with the RNA HS Assay Kit and Qubit DNA HS Assay Kit, respectively
176 (ThermoFisher Scientific). RNA and gDNA integrity were evaluated using the Bioanalyzer RNA
177 Nano Kit and DNA 1200 Kit, respectively (Agilent Technologies). Extracted RNA and gDNA were
178 stored at -80℃ and -20℃, respectively, until used.

179 **FLAIRR-seq targeted amplification of heavy chain transcripts**

180 Extracted RNA was thawed on ice and converted to first strand complementary DNA
181 (cDNA) using the SMARTer RACE 5'/3' Kit (Takara Bio USA), as described by the manufacturer
182 and a custom oligonucleotide that contained the template switch oligo and a unique molecular
183 identifier (5' TSO-UMI) for template switch during first strand cDNA synthesis. The following
184 reaction conditions were used: (i) a primary master mix was prepared with 4.0 µL 5X First-Strand
185 Buffer, 0.5 µL DTT (100 mM), and 1.0 µL dNTPs (20 mM) per reaction and set aside until needed;
186 (ii) in a separate 0.2-mL PCR tube, 10 µL of sample RNA and 1 µL 5'-CDS Primer A were
187 combined and incubated in a thermal cycler at 72°C (lid temperature: 105°C) for 3 minutes,
188 followed by cooling to 42°C for 2 minutes; (iii) after cooling, tubes were spun briefly to collect
189 contents and 1µL (12µM) of the 5' TSO-UMI was added to the RNA; (iv) 0.5 µL of RNase inhibitor
190 and 2.0 µL of SMARTScribe Reverse Transcriptase were added to the primary master mix tube
191 per sample and 8 µL of the combined master mix was then added to each RNA-containing sample
192 tube. First-strand cDNA synthesis reactions were incubated in a thermal cycler at 42°C (lid
193 temperature: 105°C) for 90 mins, followed by heat inactivation at 70°C for 10 minutes. Total first
194 strand cDNA generated in this reaction was diluted 1:2 with Tricine-EDTA Buffer before moving
195 onto targeted heavy chain transcript amplification.

196 To specifically amplify heavy chain transcripts from total first-strand cDNA, targeted IgG
197 and IgM transcript amplification reactions were performed using barcoded IgG (3' primer binding
198 in the constant region exon 3, CH3) or IgM (3' primer binding in the constant region exon 4, CH4)-
199 specific primers (Supplementary Table 2) and the following conditions: (i) 5 µL of diluted first-
200 strand cDNA was added to 0.2-mL PCR tubes; (ii) a master mix was generated using 10 µL 5X
201 PrimeSTAR GXL Buffer, 4 µL GXL dNTP mixture, 28 µL PCR-grade water, 1 µL PrimeSTAR GXL
202 Polymerase and 1 µL 10x UPM form the SMARTer RACE 5'/3' Kit per reaction; (iii) 44 µL master
203 mix was added to each reaction tube followed by 1 µL of the appropriate barcoded IgG (CH3) or
204 IgM (CH4) primer. Different temperatures were used for annealing of IgG- (63.5°C) and IgM-

205 specific primers (60°C) to account for primer specific melting temperatures and to enhance
206 targeted amplification specificity. Amplification conditions for full-length IgG were: 1 minute at
207 95°C, followed by 35 amplification cycles of 95°C for 30 sec, 63.5°C for 20 sec, and 2 minutes at
208 68°C, followed by a final extension for 3 minutes at 68°C and hold at 4°C. Amplification conditions
209 for full-length IgM were: 1 minute at 95°C, followed by 35 amplification cycles of 95°C for 30 sec,
210 60°C for 20 sec., and 2 minutes at 68°C, followed by a final extension for 3 minutes at 68°C and
211 hold at 4°C. Final amplification reactions were purified using a 1.1x (vol:vol) cleanup with ProNex
212 magnetic beads (Promega) . Successfully amplified products were quantified with Qubit dsDNA
213 HS assay (ThermoFisher Scientific) and length was evaluated with the Fragment Analyzer
214 Genomic DNA HS assay (Agilent). Samples were equimolar pooled in 8-plexes for SMRTbell
215 library preparation and sequencing.

216 **FLAIRR-seq SMRTbell library preparation and sequencing**

217 Eight-plex pools of targeted IgG or IgM amplicons were prepared into SMRTbell
218 sequencing templates according to the "Procedure and Checklist for Iso-Seq Express Template
219 for Sequel and Sequel II systems" protocol starting at the "DNA Damage Repair" step and using
220 the SMRTbell Express Template Prep Kit 2.0, with some modifications (Pacific Biosciences).
221 Briefly, targeted IgG and IgM amplicons underwent enzymatic DNA damage and end repair,
222 followed by ligation with overhang SMRTbell adapters as specified in the protocol. To increase
223 consistency in SMRTbell loading on the Sequel IIe system, we further treated the SMRTbell
224 libraries with a nuclease cocktail to remove unligated amplified products, using the SMRTbell
225 Enzyme Cleanup Kit, as recommended by the manufacturer (Pacific Biosciences). Briefly, after
226 heat-killing the ligase with an incubation at 65°C, samples were treated with a nuclease cocktail
227 at 37°C for 1 hour, and then purified with a 1.1X Pronex cleanup. Final SMRTbell libraries were
228 evaluated for quantity and quality using the Qubit dsDNA HS assay and Fragment Analyzer
229 Genomic DNA assay, respectively. Sequencing of each 8-plex, barcoded sample pool was

230 performed on one SMRTcell 8M using primer v4 and polymerase v2.1 on the Sequel IIe system
231 with 30 hr movies. Demultiplexed, high-fidelity circular consensus sequence reads ("HiFi reads")
232 were generated on the instrument for downstream analyses.

233 **AIRR-seq SMARTer Human BCR IgG/IgM sequencing**

234 Matched healthy donor RNA was used to generate targeted IgG and IgM AIRR-seq
235 libraries using the SMARTer Human BCR IgG IgM H/K/L Profiling Kit (Takara Bio USA) according
236 to the manufacturer's instructions with no modifications. Briefly, for each sample, proprietary IgG
237 and IgM primers were used to amplify heavy chain transcripts following a 5'RACE reaction. AIRR-
238 seq libraries were then quality controlled using the 2100 Bioanalyzer High Sensitivity DNA Assay
239 Kit (Agilent) and the Qubit 3.0 Fluorometer dsDNA High Sensitivity Assay Kit. Sequencing on the
240 MiSeq platform using 300 bp paired-end reads was performed using the 600-cycle MiSeq
241 Reagent Kit v3 (Illumina) according to the manufacturer's instructions, and FASTQ reads were
242 generated using the associated DRAGEN software package (Illumina).

243 **B cell Iso-Seq**

244 RNA extracted from healthy sorted B cells was used to generate Iso-Seq SMRTbell
245 libraries following the "Procedure & Checklist Iso-Seq Express Template Preparation for the
246 Sequel II System" with minor adaptations compared to the manufacturer's instructions. Briefly,
247 Iso-Seq libraries were generated using 500 ng high-quality (RIN > 8) RNA as input into oligo-dT
248 primed cDNA synthesis (NEB). Barcoded primers were incorporated into the cDNA during second
249 strand synthesis. Following double-stranded cDNA amplification, transcripts from two samples
250 sourced from purified B cells and NK cells were equimolar pooled as previously described (33).
251 SMRTbells were generated from the pooled cDNA as described above for the FLAIRR-seq
252 amplification products, including the addition of a nuclease digestion step. Quantity and quality of
253 the final Iso-Seq libraries were performed with the Qubit dsDNA High Sensitivity Assay Kit and
254 Agilent Fragment Analyzer Genomic DNA assay, respectively. This 2-plex Iso-Seq pool was

255 sequenced using primer v4 and polymerase v2.1 on the Sequel IIe system with a 30-hour movie.
256 HiFi reads were generated on instrument before analyses. Demultiplexing of barcoded samples
257 and generation of full-length non-concatemer (FLNC) predicted transcripts were performed using
258 the Iso-Seq v3 pipeline available through SMRTLink (v.10.2). B-cell-derived FLNC reads were
259 mapped to the human genome using the GMAP reference database and reads derived from
260 chromosome 14 were extracted for downstream IGH transcript characterization via Immcantation,
261 as described below.

262 **Immcantation analyses of IgG and IgM repertoires**

263 Analyses of FLAIRR-seq, AIRR-seq, and Iso-seq datasets were performed using
264 Immcantation tools (30, 31). Demultiplexed barcoded HiFi (for SMRT sequencing data) or FASTQ
265 (for AIRR-seq) reads were first processed using the pRESTO tool for quality control, UMI
266 processing, and error profiling (30). For AIRR-seq, pRESTO analysis data from paired-end reads
267 ("R1" and "R2") were trimmed to remove bases with < Q20 read quality and/or <125 bp length
268 using the "FilterSeq trimqual" and "FilterSeq length", respectively. IgG and IgM CH3 or CH4 primer
269 sequences were identified with an error rate of 0.2, and primers identified were then noted in
270 FASTQ headers using "MaskPrimers align". Next, 12 basepair (bp) UMIs were located and
271 extracted using "Maskprimers extract". Sequences found to have the same UMIs were grouped
272 and aligned using "AlignSets muscle," with a consensus sequence generated for each UMI using
273 "BuildConsensus". Mate pairing of AIRR-seq reads was conducted using a reference-guided
274 alignment requiring a minimum of a 5 bp overlap via "AssemblePairs sequential". After collapsing
275 consensus reads with the same UMI ("conscount") using "CollapseSeq"," reads with < 2
276 supporting sequences were removed from downstream analysis. For pRESTO processing of
277 FLAIRR-seq, single HiFi reads ("R1") reads did not require trimming due to > Q20 sequence
278 quality across all bases. 5'TSO-UMI and CH3 or CH4 region primers were identified along with a
279 22 bp UMI with an error rate of 0.3 using "MaskPrimers align". Reads were then grouped and

280 aligned using “AlignSets muscle”. Due to the single molecule nature of FLAIRR-seq reads, no
281 mate pairing was required. Consensus reads were then generated as described above, including
282 removal of sequences with < 2 supporting reads. Read counts following each step of data filtration
283 for AIRR-seq and FLAIRR-seq are represented in Supplementary Tables 3 and 4, respectively.

284 pRESTO-filtered reads for both AIRR-seq and FLAIRR-seq data were then input into the
285 Change-O tool (Table 1). Iso-seq required no initial processing from pRESTO and was input into
286 Change-O for IG gene reference alignment along with AIRR-seq and FLAIRR-seq data using
287 “igblastn”, clonal clustering using “DefineClones”, and germline reconstruction and conversion
288 using “CreateGermlines.py” and the GRCh38 chromosome 14 germline reference (31). Fully
289 processed and annotated data was then converted into a TSV format for use in downstream
290 analyses. The Alakazam Immcantation tool suite was then used to quantify gene usage analysis,
291 calculate CDR3 length, assess somatic hypermutation frequencies, and analyze clonal diversity
292 (31). SCOPer clonal assignment by spectral clustering was conducted for COVID-19 patient time
293 course samples (34, 35). For clonal lineage tree analysis, the Dowser tool was used to examine
294 clonal diversity and CSR over time (36).

295 **Targeted IG gDNA capture, long-read sequencing, and IGenotyper analyses.**

296 FLAIRR-seq validation samples also underwent IGHC targeted enrichment and long-read
297 sequencing as previously described (37). Briefly, gDNA was mechanically sheared and size
298 selected to include 5-9kb fragments using the BluePippin (Sage Science). Samples were then
299 end repaired and A-tailed using the standard KAPA library preparation protocol (Roche).
300 Universal priming sequences and barcodes were then ligated onto samples for multiplexing
301 (Pacific Biosciences). Barcoded gDNA libraries were captured using IGH-specific probes
302 following a SeqCap protocol (Roche). 26 IGH-enriched samples were purified and pooled together
303 for SMRTbell library prep as described above, including the final nuclease digestion step. Pooled
304 SMRTbells were annealed to primer v4, bound to polymerase v2.0, and sequenced on the Sequel

305 IIe system with 30h movies. After sequencing, HiFi reads were generated and analyzed by the
306 IGenotyper pipeline (37). In brief, IGenotyper was used to detect single nucleotide variants and
307 assemble sequences into haplotype-specific assemblies for downstream IGHC gene genotyping.
308 Alleles were then extracted from assemblies using a bed file containing coordinates for each
309 IGHC gene exon. After sequences were extracted, reads were then aligned to the IMGT database
310 (downloaded on 2/21/22) and assigned as an exact match to IMGT, "novel" if there was no match
311 to the IMGT database or "novel, extended" if a match was detected to a partial allele found in
312 IMGT, but the IMGT allele was a substring of the IGenotyper identified allele (38). This set of
313 alleles was then used as a ground truth dataset.

314 **IGHC gene genotyping with FLAIRR-seq**

315 To genotype IGHC genes and alleles from FLAIRR-seq data, productive reads were
316 filtered by IGHC length (900bp–1100bp) and aligned to the chromosome 14 hg38 reference using
317 minimap2 along with SAMtools to generate sorted and indexed bam files (39, 40). WhatsHap was
318 used to identify, genotype, and phase single nucleotide variants (SNV) (41). Phased SNVs were
319 used to assign each read to a haplotype using MsPAC. Reads from each haplotype and gene
320 were clustered using CD-HIT using a 100% identity clustering threshold parameter, and a single
321 representative read from the largest cluster was aligned to the IGenotyper curated alleles using
322 BLAST (42) to determine the closest matching IGHC gene and allele (38, 43). The representative
323 read was selected based on 100% identity to all other sequences in that cluster.

324 **Inference of IGHV, IGHD, and IGHJ gene haplotypes from FLAIRR-seq data using IGHC**
325 **gene anchors**

326 To test the ability of IGHC genes to be used for the inference of IGHV, IGHD, and IGHJ haplotypes
327 from FLAIRR-seq data, we chose one sample that was heterozygous for both IGHM and IGHJ6
328 (IGHJ6 is standardly used for AIRR-seq haplotype inference). For this sample, we employed
329 TigGER (31, 44-46) to infer novel IGHV alleles, and generate sample-level IGHV genotypes using

330 a Bayesian approach. Rearranged sequences within the Change-O table were then reannotated
331 taking into account sample genotype and detected novel alleles. Updated annotations were then
332 used to infer haplotypes using RAbHIT version 0.2.4 (47). Both IGHJ6 and IGHM were used as
333 anchor points for haplotyping, and the resulting haplotypes were compared.

334 **Results**

335 **Gene usage, CDR3, and SHM profiles characterized from FLAIRR-seq data are comparable**
336 **to AIRR-seq and Iso-Seq**

337 Current methods for commercially available 5' RACE AIRR-Seq utilize targeted
338 amplification of the variable region and, in some cases, a small portion of the first constant region
339 exon (CH1), in conjunction with short-read sequencing to characterize IG repertoires. However,
340 this minimal examination of the IGHC gene sequence is primarily used to define isotypes. No
341 current method defines both the heavy chain variable and constant regions allowing for both
342 subisotype classification and IGHC allele-level resolution. To address these technical limitations,
343 we developed the FLAIRR-Seq method (Figure 1C), a targeted 5' RACE approach combined with
344 SMRT sequencing to generate highly accurate, near full-length IgG (~1500 bp) and/or IgM (2000
345 bp) sequences, allowing for direct, simultaneous analysis of the heavy chain variable and constant
346 regions (Figure 1D), including gene/allele identification for IGHV, IGHD, IGHJ and IGHC
347 segments, and isotype- and subisotype-specific repertoire profiling.

348 To evaluate and validate the capabilities of FLAIRR-seq, matched FLAIRR-seq and AIRR-
349 seq analyses were performed on ten healthy donor PBMC samples. FLAIRR-seq data were
350 filtered from the initial HiFi reads (>Q20) to include only >Q40 reads. The average read quality of
351 these filtered reads was >Q60 (99.9999%), with a pass filter rate ranging from 88%-93% of total
352 reads. AIRR-seq FASTQ bases were trimmed to retain sequences with an average quality of Q20
353 (99%). These filtered reads were used as input into the Immcantation suite, specifically the
354 pREST-O and Change-O tools, for IGHV, IGHD, and IGHJ gene assignment, and repertoire

355 feature analyses, including identification of clones, extent of somatic hypermutation, and
356 evaluation of CDR3 lengths. As shown in **Table 1,** fewer overall FLAIRR-seq reads were used as
357 input into the Immcantation analyses, after required filtration and read assembly steps (which
358 were not needed for the high-quality single-molecule FLAIRR-seq reads). FLAIRR-seq resulted
359 in comparable or, in many cases, increased number of unique VDJ sequences, clones, and CDR3
360 sequences identified compared to the matched AIRR-seq-derived samples in both the IgG and
361 IgM repertoires. These basic sequencing and initial analysis metrics demonstrated that FLAIRR-
362 seq produced high-quality variable region data for detailed Ab repertoire analyses and is
363 amenable to analysis using existing AIRR-seq analysis tools. While input RNA mass used for
364 FLAIRR-seq was often more than for AIRR-seq, ongoing and future optimization of the method is
365 aimed at reducing RNA input. Furthermore, a comparative cost analysis was performed. To obtain
366 the closest metric to a direct comparison, we calculated the cost per "actionable read", defined as
367 the read number per sample and per method after read and length quality filtration and assembly,
368 but prior to cluster consensus, performed in the pRESTO pipeline. This method was used to
369 represent the total unique single molecule or assembled templates captured by either the
370 FLAIRR-seq or AIRR-seq methods, respectively, that passed all necessary quality control criteria
371 for downstream annotation and analyses irrespective of biologic repertoire diversity or clonality.
372 Lastly, to remove the impact of pooling differences, we used this "per actionable read" cost to
373 calculate the cost for the generation of 15,000 "actionable reads" as our standard price. For AIRR-
374 seq this cost was $25.50 per sample, whereas for FLAIRR-seq, this cost was $33.57 per sample.
375 These costs reflect needed reagents and consumables only, assume instrumentation access and
376 do not include labor. Future optimization for FLAIRR-seq will include integrating a multiplexed
377 array sequencing (MAS) step to concatenate reads and enhance overall depth of sequencing and
378 multiplexing capacity per pool, resulting in decreasing costs per sample (48).

379 While optimizing FLAIRR-seq sample preparation, we examined whether upstream
380 isolation of B cells before FLAIRR-seq molecular preparation would enhance the ability to detect
381 IGHV, IGHD, and IGHJ gene usage. To do this, aliquots of PBMC (n=4) were split into two groups
382 for RNA extraction: (i) RNA derived from bulk PBMC, and (ii) RNA isolated from purified pan B-
383 cells, followed by FLAIRR-seq preparation, SMRT sequencing, and Immcantation analysis of both
384 groups. IGHV, IGHD, and IGHJ gene usage correlations between groups are shown in Figure 2A
385 and demonstrate a significant association (p-values ranging from 0.033 to $4.1e^{-16}$) strongly
386 supporting the conclusion that B cell isolation before RNA extraction was not necessary to achieve
387 comparable gene usage metrics. The limited differences that were observed could be explained
388 by template sampling differences between the two experiments. Due to the strong associations
389 observed and the ease of processing PBMC in bulk, we moved forward with RNA derived directly
390 from PBMC aliquots for the remainder of our analyses.

391 We established FLAIRR-seq performance by comparing its output to the commonly used
392 5' RACE AIRR-seq method. 5' RACE AIRR-seq was chosen as it provides resolution of the
393 complete variable region and a small portion of IGHC, allowing for isotype differentiation.
394 Following matched preparation of both FLAIRR-seq and AIRR-seq libraries from healthy donor
395 PBMC samples (n=10), we compared multiple repertoire features to benchmark FLAIRR-seq
396 performance. First, we evaluated IGHV, IGHD, and IGHJ gene usage frequencies. We observed
397 significant correlations between FLAIRR-seq and AIRR-seq datasets in IGHV, IGHD and IGHJ
398 gene usage for both IgM (V genes: r = 0.93-0.97, $p=<2.2e^{-16}$; D genes: r = 0.98-0.99, $p=<2.2e^{-16}$;
399 J genes: r = 0.94-1.0, p = 0.0028-0.017) and IgG isotypes (V genes: r = 0.90-0.96, $p=<2.2e^{-16}$; D
400 genes: r = 0.87-0.99, $p=<2.2e^{-16}$-$6.1e^{-14}$;J genes: r = 0.89-1.0, p = 0.0028-0.033) (Figure 2B),
401 indicating that FLAIRR-seq comparably resolves IGHV, IGHD, and IGHJ gene usage profiles. To
402 note, IGHJ genes showed lower levels of significance (larger p-values) across all comparisons
403 due to the relatively few genes that make up the IGHJ gene family compared to the more diverse

404 IGHV and IGHD families. We next investigated the performance of both methods in terms of
405 resolving somatic hypermutation (SHM) frequencies (Figure 2C), and complementarity
406 determining region 3 (CDR3) lengths (Figure 2D), which are often used as measures of evaluating
407 B cell affinity maturation. Although we did observe occasional statistically significant differences
408 in the SHM frequency between AIRR-seq and FLAIRR-seq data using the same samples, these
409 differences were not seen across all samples, suggesting that sample-to-sample variation may
410 drive this observation rather than technology-based discrepancies. We found that CDR3 lengths
411 were consistently longer in the FLAIRR-seq datasets for both the IgM and IgG isotypes in most
412 donors. The characterization of unusually long CDR3 regions (> 40 nt) in the IgG sequences with
413 FLAIRR-seq is likely due to the higher contiguity and quality afforded by the longer read lengths,
414 which are less likely to be spanned by short-read 2x300 bp paired-end sequencing strategies.
415 Together, these data demonstrate that FLAIRR-seq achieves comparable gene usage profiles,
416 and improved resolution of long CDR3 sequences.

417 Others have recognized the power of long-read sequencing to resolve B cell repertoires
418 using bulk Iso-Seq methods, allowing for the examination of full-length transcripts from isolated B
419 cells (49). The Iso-Seq method captures full-length transcripts expressing a poly(A) tail without
420 bias through oligo dT-based priming. The trade-offs of this approach are throughput, depth, and
421 cost, as Iso-Seq processing generates a complete transcriptome per sample without enrichment
422 of heavy chain sequences, which then need to be filtered out and analyzed, resulting in a
423 considerable amount of non-repertoire data that is discarded. To investigate whether the
424 untargeted transcriptome-wide Iso-Seq method would resolve a qualitatively different repertoire
425 than FLAIRR-seq, which would have indicated FLAIRR-seq-driven primer bias, we performed
426 matched Iso-Seq and FLAIRR-seq on purified B-cell derived RNA. IGHV, IGHD, and IGHJ gene
427 usage frequencies were compared between Iso-Seq and FLAIRR-seq datasets (Spearman's rank
428 correlation), revealing significant correlations between usage profiles (V genes: $r = 0.94$, $p=2.2e^{-}$

429 [16]; D genes: r = 0.92, p =1.4e^{-13}; J genes: r = 1.0, p = 0.0028; Figure 2E). These data strongly
430 suggest that FLAIRR-seq has very limited to no primer-driven bias compared to whole
431 transcriptome data. Collectively, this benchmarking dataset confirmed that FLAIRR-seq is
432 comparable other state-of-the-art methods, providing robust characterization of commonly used
433 repertoire metrics, with limited increases in per sample cost.

434 **IGenotyper and FLAIRR-seq provide constant region gene allele identification and allow**
435 **for haplotyping of variable genes**

436 The novel value added by FLAIRR-seq is improved resolution of IGHC, including
437 estimation of IGHC gene and allele usage, subisotype identification, and phasing of variable and
438 constant regions for comprehensive repertoire analysis**.** To evaluate the capabilities and accuracy
439 of IGHC gene and allele identification with FLAIRR-seq, we first established a ground truth dataset
440 of IGHC alleles for all 10 samples by targeted sequencing of the germline IGH locus (Figure 3A)
441 using IGenotyper, as previously described (37). IGHG1, IGHG2, IGHG3, IGHG4 and IGHM alleles
442 called by IGenotyper (see Methods) were assigned to one of three categories, schematized in
443 Figure 3B: (i) “exact match” - alleles documented in the IMGT database; (ii) “novel not in IMGT”
444 – alleles not documented in the IMGT database; or (iii) “extended” – alleles that matched partial
445 alleles in the IMGT database (i.e., those only spanning a subset of exons), but were extended by
446 sequences in our dataset. IGenotyper identified a total of 32 unique IGHG1, IGHG2, IGHG3,
447 IGHG4 and IGHM alleles across all individuals, as schematized in Figure 3C. Among these 32
448 alleles, only 4 were documented in IMGT, the remaining represented novel alleles (n=11) or
449 extensions (n=17) of known alleles. In aggregate, we observed a greater number of IGHG4 alleles
450 than for any of the IGHG genes. Among these alleles were 4 sequences represented by
451 suspected duplications of IGHG4. In fact, we observed 3 IGHG4 gene alleles in 4/10 samples,
452 indicating the presence of gene duplications in these donors; in all cases, these alleles were also
453 identified in the FLAIRR-seq data (see below). Given the relatively small size of this proof-of-

454 concept healthy donor cohort, the identification of 28 (87%) novel or extended alleles underscores
455 the extensive polymorphism In this region and reflects the paucity of information regarding this
456 locus in existing immunogenomics databases.

457 We next used the iGenotyper-derived IGHC gene database as the ground-truth for
458 evaluating the capability of FLAIRR-seq to identify and resolve IGHC gene alleles. Based on our
459 analysis workflow for identifying IGHC alleles from FLAIRR-seq data, we resolved 19/32 (59%)
460 iGenotyper alleles at 100% identity; no additional false-positive alleles were identified. Of the
461 alleles that were not unambiguously resolved by our FLAIRR-seq pipeline, 8 had allele defining
462 single nucleotide variants (SNVs) 3' of the FLAIRR-seq primers. The rate of true-positive allele
463 calls using FLAIRR-seq across all 10 samples ranged from 5% for IGHG1 to 90% for IGHM
464 (Figures 3C and 3D). As a result, the IGHC genotypes inferred by FLAIRR-seq have some
465 limitations, but on the whole allow for much greater resolution of IGHC variation in the expressed
466 repertoire than currently used methods. Future iterations of FLAIRR-seq will include primer
467 optimization to facilitate better sequence coverage in the 3' regions of the IGHC alleles and
468 improve the direct genotyping capabilities of the FLAIRR-seq method.

469 Previous studies have demonstrated the use of IGHJ6 heterozygosity to infer haplotypes
470 of V and D genes from AIRR-seq data (46, 50). However, the frequency of IGHJ6 heterozygotes
471 in the population can vary. Therefore, we wanted to assess the utility of leveraging IGHC
472 polymorphism resolved by FLAIRR-seq for haplotyping IGHV alleles with the publicly available
473 tool RAbHIT(46, 50, 51). We selected a single donor ("1013") from our cohort that was
474 heterozygous for both IGHJ6 (*02 and *03) and IGHM (FL_2 and FL_4). Importantly, we were
475 able to associate each IGHJ6 allele to the respective IGHM allele from the corresponding
476 haplotype (Figure 3E). After defining germline IGHV alleles using TIgGER (31), we generated and
477 compared IGHV haplotype inferences using either IGHJ6 or IGHM alleles as anchor genes using
478 RAbHIT (47)(Figure 3E). Although some allele assignments were ambiguous ("unknown") using

479 both methods, we observed a strong consensus between haplotype inferences using the two
480 anchor genes. For haplotype 1, represented by IGHJ6*03 and IGHM_FL_4, the IGHJ6*03-derived
481 haplotype had 35 IGHV genes for which either an allele or deletion call was made. When using
482 IGHM_FL_4, the same allele/deletion calls were made for 33 of these genes; in addition, using
483 IGHM as the anchor gene, assignments were made for an additional 5 IGHV genes that had
484 "unknown" designations using IGHJ6. Similarly, of the allele/deletion calls made for 36 IGHV
485 genes on haplotype 2 assigned to IGHJ6*02, 33 of these gene had identical assignments to
486 IGHM_FL_2. Together these results indicate that IGHC variants can be utilized for haplotype
487 inference from repertoire data when commonly used IGHJ or IGHD genes are homozygous in
488 individuals of interest.

489 **FLAIRR-seq enables isotype-, subisotype-, and allele-specific repertoire analyses**

490 IGHG and IGHM alleles identified in each sample were used to annotate reads in each
491 respective repertoire. These assignments allowed for partitioning of the repertoire by isotype,
492 subisotype and IGHC allele (Figure 4). To demonstrate this, we utilized the same represtentative
493 sample ("1013") that was heterozygous for all IGHC genes. As shown in Figure 4A, IGHC gene
494 assignments allow for subisotype and allele level frequencies to be estimated as a proportion of
495 the overall IgG and IgM repertoires. In addition, detailed analyses of the repertoire can be
496 conducted within each of these compartments. For example, Figure 4B shows the frequencies of
497 IGHV gene subfamilies for each IGHG and IGHM allele identified in this sample. Using standard
498 AIRR-seq analyses, we would not be able to identify allele-resolved V gene usage or enrichment
499 within subisotype populations, which is important for linking subisotype functionality to particular
500 antigen-specific VDJ clones.

501 Through the partitioning of repertoire sequences by subisotype and IGHC allele, we found
502 that FLAIRR-seq also allowed for trends to be assessed in aggregate across donors. To
503 demonstrate this, we further examined V gene family usage partitioned by IgG subisotype across

504 all 10 healthy donors. This analysis revealed expected patterns, in that IGHV1, IGHV3 and IGHV4
505 subfamily genes were dominant across the 4 subisotypes (Figure 4C). However, we did observe
506 significant variation in subfamily proportions between subisotypes, associated with distinct
507 profiles in specific subisotypes (Figure 4C). Specifically, the estimated frequencies of IGHV1 and
508 IGHV3 were statistically different between subisotypes ($P<0.01$, ANOVA); IGHV1 usage was
509 elevated in IGHG1 and IGHG4, whereas IGHV3 was elevated in IGHG2 and IGHG3. These
510 analyses demonstrate the unique capability of FLAIRR-seq to examine variation in the expressed
511 repertoire at the level of isotype, subisotype, and IGHC allele. As samples sizes increase, we
512 expect that a multitude of additional repertoire features will become accessible to this kind of
513 analysis leading to novel discoveries linking VDJ and IGHC genetic signatures.

514 **FLAIRR-seq identifies subisotype-specific clonal expansion and CSR in longitudinal**
515 **samples.**

516 We wanted to investigate the utility of FLAIRR-seq in clinical samples, particularly to
517 observe changes in immune repertoires over time. Ab responses are highly dynamic, with specific
518 Ab clones expanding upon activation by antigen. We were interested to know if class switch
519 recombination could be captured by FLAIRR-seq, given the capability to identify clones with the
520 subisotype resolved. We had the opportunity to evaluate FLAIRR-seq resolved repertoires over
521 time in four samples collected from one individual over their >13-day hospitalization for severe
522 COVID-19 disease. Blood draws were taken on days 1, 4, 8, and 13 post-hospitalization (Figure
523 5A) and analyzed with FLAIRR-seq across all time points. After initial FLAIRR-seq processing
524 and analysis, we defined unique clones using SCOPer, which clusters sequences based on CDR3
525 similarity and mutations in IGHV and IGHJ genes (34). This analysis allowed for the estimation of
526 subisotype-specific clone counts across the four timepoints examined. Overall, we observed IgG1
527 dominated the repertoire at all four time points, but the proportion of subisotypes fluctuated over
528 time (Figure 5B). Specifically, the IGHG2 and IGHG3-specific repertoires expanded from day 1 to

529 day 4, but then contracted in overall frequency from day 8 to day 13 (Figure 5B). To assess clonal
530 diversity within each subisotype repertoire across time, we calculated the Simpson's diversity
531 index (q=2) using Alakazam (31). All subisotype-specific repertoires became less diverse from
532 day 1 to day 4, suggesting clonal expansion across the IGHG repertoire (Figure 5C). To note,
533 IGHG4 was not included in diversity calculations because IGHG4 would have required higher
534 sequencing depth to ascertain diversity, given the overall lower expression of IgG4 transcripts in
535 this individual. Subisotype-specific repertoire polarity was also assessed by calculating the
536 fraction of clones needed to represent 80% of the total repertoire (Figure 5D), with lower fractions
537 representing more polarized and clonally expended repertoires. Results of this analysis were
538 consistent with the diversity index, demonstrating an increase in clonal expansion (i.e., decreased
539 polarity) at day 4 across IGHG1, IGHG2, and IGHG3 compartments, which returned to baseline
540 at later timepoints.

541 CSR mediates the switching of Abs from one sub/isotype to another. This occurs through
542 the somatic recombination of IGHC genes, which brings the switched/selected IGHC genes
543 adjacent to the recombined IGHV, IGHD, and IGHJ segments, facilitating transcription. The
544 switching of isotypes and subisotypes can result in changes to associated effector functions of
545 the Ab while maintaining antigen-specific variable regions. Given the ability of FLAIRR-seq to
546 resolve clones with subisotype and IGHC allele resolution, as proof-of-concept, we sought to
547 assess whether FLAIRR-seq could allow for more detailed haplotype-level analysis of CSR
548 through the course of infection. To do this, we identified the largest clones in our dataset that were
549 both represented by multiple isotypes and found across timepoints. In total, using SCOper (34),
550 we identified 19 unique clonal lineages that met this criteria. We focused our detailed analysis on
551 one of the largest clones, "9900" (Figure 5E), comprising IGHM, IGHG1, and IGHG2 sequences.
552 On day 1 post-hospitalization, clone 9900 sequences were represented by both IGHM and
553 IGHG2. At day 4, IGHG2 was the only isotype observed, whereas again at day 8, both IGHM and

554 IGHG2 were observed, as well as IGHG1. To visualize CSR, we built a phylogeny using Dowser
555 (36). Highlighted in the red box on the phylogenetic tree shown in Figure 5F, we observe a single
556 subclade that is represented by IGHM, IGHG1, and IGHG2.

557 We were also able to resolve IGHC alleles from this individual, with the exception of
558 IGHG1 alleles which were ambiguous. Critically, both IGHG1 and IGHG2 were heterozygous
559 (Figure 5G). Through the assignment IGHG alleles to haplotypes within this individual using
560 heterozygous V genes (IGHV3-7 and IGHV3-48), we were able to determine that sequences from
561 clone 9900 (Figure 5F) utilized IGHG1 and IGHG2 alleles from the same haplotype, associated
562 with IGHV3-7*07 and IGHV3-48*03 (31). This observation offers direct characterization of CSR
563 events occurring on the same chromosome. When we looked across the remaining clones (n=8)
564 in this dataset that spanned time points and were represented by IGHG1 and IGHG2 subisotypes,
565 we were able to confirm that all of these clones used IGHG alleles from the same haplotype.

566 Together, these data provide demonstrative proof-of-concept evidence that FLAIRR-seq
567 profiling performs robustly on clinical samples, including RNA directly extracted from whole blood.
568 In addition, these data provide novel repertoire resolution extending what would have been
569 possible with standard AIRR-seq methods, including analysis of subisotype-specific repertories,
570 evaluation of clonal expansion, and characterization of CSR in the IgG and IgM repertoires.

571 **Discussion**

572 Here we present the development, validation, and application of FLAIRR-seq, a novel
573 method to resolve near full-length Ab transcripts from bulk PBMC-, isolated B cell- and whole
574 blood-derived total RNA. FLAIRR-seq enables highly accurate, simultaneous resolution of
575 variable and constant regions and suggests that IGHC polymorphism is far more extensive than
576 previously assumed. FLAIRR-seq performed equivalent to or with increased resolution compared
577 to existing standard 5'RACE AIRR-seq methods when resolving V, D, and J gene calls, CDR3
578 lengths, and SHM signatures, suggesting that our CH3/CH4 targeting strategies did not

579 compromise variable region characterization while simultaneously adding the capability to resolve
580 IGHC variation. Little to no primer bias was observed when compared to Ab repertoire profiling
581 from total mRNA Iso-seq methods. FLAIRR-seq provides the novel ability to use IGHC gene
582 usage to identify subisotypes and genotype heavy chain transcripts, linking these data back to
583 evaluate subisotype-specific repertoires, clonal expansion, and CSR. Underscoring the
584 underappreciated extent of IGHC variation, our profiling of a restricted cohort of only 10 individuals
585 from relatively homogenous backgrounds still identified 4 and 7 completely novel IGHC alleles in
586 IgM and IgG, respectively, and extended an additional 17 alleles beyond which had been available
587 in the IMGT database.

588 The unique capabilities of FLAIRR-seq will allow for novel examination of Ab repertoires,
589 including the characterization of variable gene usage and clonotype distribution within unique
590 subisotype subsets. This perspective has the potential to provide key insights into dynamic Ab
591 responses in diseases known to be mediated by subisotype-specific processes or have skewed
592 subisotype distribution as predictive markers of disease, including Myasthenia gravis (mediated
593 by pathogenic autoantibodies across subisotypes that give rise to varied disease pathologies),
594 Acute Rheumatic Fever (associated with elevated IgG3), and melanoma (skewing towards IgG4
595 in late-stage disease thought to be indicative of tolerogenic responses and poor prognosis)(12-
596 14). These subisotype-specific repertoire profiling approaches may be the first step toward
597 identification of unique clones that mediate disease pathogenicity or serve as high-resolution
598 biomarkers to disease progression, as well as open the door for potential functional experiments
599 on subisotype clones of interest, including examining the functional impact of the novel IGHC
600 alleles identified here. Expanded population-based FLAIRR-seq profiling and curation of novel
601 IGHC alleles, particularly in conjunction with IGenotyper targeted genomic assembly efforts in
602 IGH, will be a significant first step in defining the full extent of variation in a region too long
603 assumed to be relatively invariant.

604 The Fc region is known to be critical for modulating differential Ab effector functions. These
605 differential functionalities are currently understood to be regulated by differential posttranslational
606 modifications, such as variable glycosylation (52-55). Future FLAIRR-seq profiling will be a
607 valuable tool to investigate how genomic variation across IGHC genes impacts residue usage
608 and resultant Fc receptor binding, signaling potential, crosslinking, and potential for
609 posttranslational modification, all of which would be expected to alter downstream effector
610 functions, such as ADCC, ADCP, and complement fixation.

611 We further demonstrate that FLAIRR-seq can effectively examine clonal expansion and
612 CSR in longitudinal samples, demonstrating the feasibility of using FLAIRR-seq to resolve Ab
613 repertoire dynamics. This increased resolution will further our understanding of Ab repertoire
614 evolution in the transition of acute to chronic disease states, many of which are associated with
615 overall IgG subisotype distribution changes that are thought to reflect the inflammatory milieu (14,
616 56). One example is advanced melanoma, where late-stage disease is characterized by elevated
617 IgG4 compared to IgG1, which is believed to reflect a more tolerizing, pro-tumor environment (12).
618 FLAIRR-seq examination of these samples may identify specific repertoire distribution patterns
619 that could act as biomarkers of disease progression. Moving forward it is critical to account for all
620 variability within the Ab repertoire for the most comprehensive understanding of repertoire
621 dynamics and the myriad factors impacting Ab effector function. Future efforts will expand
622 FLAIRR-seq methods to target IGHA and IGHE repertoires, as well as implement multiplexed
623 arrays (MAS) sequencing to considerably increase throughput and lower cost (48). Together, the
624 data presented here demonstrate that the FLAIRR-seq method provides a comprehensive
625 characterization of allele-resolved IgG and IgM repertoires, detailing variable region gene usage
626 and measurements of maturation, isotype and subisotype identification, and the unappreciated
627 extent of constant region variation, which will be necessary to fully appreciate the impact of IG
628 genomic variation in health and disease.

Acknowledgements:

The authors would like to thank Kamille Rasche, Kaitlyin Shields, Uddalok Jana, and the staff of the University of Louisville Sequencing Technology Center for assistance in the sequencing and analysis of FLAIRR-seq samples. They would also like to acknowledge the support and assistance from Gur Yaari and Ayelet Peres for their assistance with the RabHIT workflow. This work was funded, in part, by P20 GM135004-02 (EEF, DT, CTW, and MLS).

636 **References:**

637 1. Schroeder, H. W., and L. Cavacini. 2010. Structure and function of immunoglobulins.
638 *Journal of Allergy and Clinical Immunology* 125: S41-S52.

639 2. Janda, A., A. Bowen, N. S. Greenspan, and A. Casadevall. 2016. Ig Constant Region
640 Effects on Variable Region Structure and Function. *Front Microbiol* 7: 22.

641 3. Nakano, T., M. Matsui, I. Inoue, T. Awata, S. Katayama, and T. Murakoshi. 2011. Free
642 immunoglobulin light chain: Its biology and implications in diseases. *Clinica Chimica Acta*
643 412: 843-849.

644 4. Lu, L. L., T. J. Suscovich, S. M. Fortune, and G. Alter. 2018. Beyond binding: antibody
645 effector functions in infectious diseases. *Nature Reviews Immunology* 18: 46-61.

646 5. Vidarsson, G., G. Dekkers, and T. Rispens. 2014. IgG subclasses and allotypes: from
647 structure to effector functions. *Front Immunol* 5: 520-520.

648 6. Greiff, V., C. R. Weber, J. Palme, U. Bodenhofer, E. Miho, U. Menzel, and S. T. Reddy.
649 2017. Learning the High-Dimensional Immunogenomic Features That Predict Public and
650 Private Antibody Repertoires. *The Journal of Immunology* 199: 2985.

651 7. Tonegawa, S. 1983. Somatic generation of antibody diversity. *Nature* 302: 575-581.

652 8. Nishana, M., and S. C. Raghavan. 2012. Role of recombination activating genes in the
653 generation of antigen receptor diversity and beyond. *Immunology* 137: 271-281.

654 9. Tong, P., A. Granato, T. Zuo, N. Chaudhary, A. Zuiani, S. S. Han, R. Donthula, A.
655 Shrestha, D. Sen, J. M. Magee, M. P. Gallagher, C. E. van der Poel, M. C. Carroll, and D.
656 R. Wesemann. 2017. IgH isotype-specific B cell receptor expression influences B cell fate.
657 *Proc Natl Acad Sci U S A* 114: E8411-e8420.

658 10. Noviski, M., J. L. Mueller, A. Satterthwaite, L. A. Garrett-Sinha, F. Brombacher, and J.
659 Zikherman. 2018. IgM and IgD B cell receptors differentially respond to endogenous
660 antigens and control B cell fate. *eLife* 7: e35074.

661 11. Stavnezer, J., J. E. Guikema, and C. E. Schrader. 2008. Mechanism and regulation of
662 class switch recombination. *Annu Rev Immunol* 26: 261-292.
663 12. Karagiannis, P., A. E. Gilbert, D. H. Josephs, N. Ali, T. Dodev, L. Saul, I. Correa, L.
664 Roberts, E. Beddowes, A. Koers, C. Hobbs, S. Ferreira, J. L. Geh, C. Healy, M. Harries,
665 K. M. Acland, P. J. Blower, T. Mitchell, D. J. Fear, J. F. Spicer, K. E. Lacy, F. O. Nestle,
666 and S. N. Karagiannis. 2013. IgG4 subclass antibodies impair antitumor immunity in
667 melanoma. *J Clin Invest* 123: 1457-1474.
668 13. Chung, A. W., T. K. Ho, P. Hanson-Manful, S. Tritscheller, J. M. Raynes, A. L. Whitcombe,
669 M. L. Tay, R. McGregor, N. Lorenz, J. R. Oliver, J. K. Gurney, C. G. Print, N. J. Wilson,
670 W. J. Martin, D. A. Williamson, M. G. Baker, and N. J. Moreland. 2020. Systems
671 immunology reveals a linked IgG3-C4 response in patients with acute rheumatic fever.
672 *Immunol Cell Biol* 98: 12-21.
673 14. Vander Heiden, J. A., P. Stathopoulos, J. Q. Zhou, L. Chen, T. J. Gilbert, C. R. Bolen, R.
674 J. Barohn, M. M. Dimachkie, E. Ciafaloni, T. J. Broering, F. Vigneault, R. J. Nowak, S. H.
675 Kleinstein, and K. C. O'Connor. 2017. Dysregulation of B Cell Repertoire Formation in
676 Myasthenia Gravis Patients Revealed through Deep Sequencing. *J Immunol* 198: 1460-
677 1473.
678 15. Huijbers, M. G., L. A. Querol, E. H. Niks, J. J. Plomp, S. M. van der Maarel, F. Graus, J.
679 Dalmau, I. Illa, and J. J. Verschuuren. 2015. The expanding field of IgG4-mediated
680 neurological autoimmune disorders. *European Journal of Neurology* 22: 1151-1161.
681 16. Polonelli, L., J. Pontón, N. Elguezabal, M. D. Moragues, C. Casoli, E. Pilotti, P. Ronzi, A.
682 S. Dobroff, E. G. Rodrigues, M. A. Juliano, D. L. Maffei, W. Magliani, S. Conti, and L. R.
683 Travassos. 2008. Antibody complementarity-determining regions (CDRs) can display
684 differential antimicrobial, antiviral and antitumor activities. *PLoS One* 3: e2371.

685 17. Liu, H., W. Pan, C. Tang, Y. Tang, H. Wu, A. Yoshimura, Y. Deng, N. He, and S. Li. 2021.
686 The methods and advances of adaptive immune receptors repertoire sequencing.
687 *Theranostics* 11: 8945-8963.
688 18. Trück, J., A. Eugster, P. Barennes, C. M. Tipton, E. T. Luning Prak, D. Bagnara, C. Soto,
689 J. S. Sherkow, A. S. Payne, M.-P. Lefranc, A. Farmer, A. C. The, M. Bostick, and E.
690 Mariotti-Ferrandiz. 2021. Biological controls for standardization and interpretation of
691 adaptive immune receptor repertoire profiling. *eLife* 10: e66274.
692 19. Horns, F., C. Vollmers, D. Croote, S. F. Mackey, G. E. Swan, C. L. Dekker, M. M. Davis,
693 and S. R. Quake. 2016. Lineage tracing of human B cells reveals the in vivo landscape of
694 human antibody class switching. *eLife* 5: e16578.
695 20. Calonga-Solís, V., D. Malheiros, M. H. Beltrame, L. d. B. Vargas, R. M. Dourado, H. C.
696 Issler, R. Wassem, M. L. Petzl-Erler, and D. G. Augusto. 2019. Unveiling the Diversity of
697 Immunoglobulin Heavy Constant Gamma (IGHG) Gene Segments in Brazilian
698 Populations Reveals 28 Novel Alleles and Evidence of Gene Conversion and Natural
699 Selection. *Front Immunol* 10.
700 21. Jonsson, S., G. Sveinbjornsson, A. L. de Lapuente Portilla, B. Swaminathan, R. Plomp,
701 G. Dekkers, R. Ajore, M. Ali, A. E. H. Bentlage, E. Elmér, G. I. Eyjolfsson, S. A.
702 Gudjonsson, U. Gullberg, A. Gylfason, B. V. Halldorsson, M. Hansson, H. Holm, Å.
703 Johansson, E. Johnsson, A. Jonasdottir, B. R. Ludviksson, A. Oddsson, I. Olafsson, S.
704 Olafsson, O. Sigurdardottir, A. Sigurdsson, L. Stefansdottir, G. Masson, P. Sulem, M.
705 Wuhrer, A.-K. Wihlborg, G. Thorleifsson, D. F. Gudbjartsson, U. Thorsteinsdottir, G.
706 Vidarsson, I. Jonsdottir, B. Nilsson, and K. Stefansson. 2017. Identification of sequence
707 variants influencing immunoglobulin levels. *Nature Genetics* 49: 1182-1191.
708 22. Buck, D., E. Albrecht, M. Aslam, A. Goris, N. Hauenstein, A. Jochim, S. Cepok, V.
709 Grummel, B. Dubois, A. Berthele, P. Lichtner, C. Gieger, J. Winkelmann, and B. Hemmer.

710 2013. Genetic variants in the immunoglobulin heavy chain locus are associated with the
711 IgG index in multiple sclerosis. *Ann Neurol* 73: 86-94.
712 23. Keyeux, G., G. Lefranc, and M.-P. Lefranc. 1989. A multigene deletion in the human IGH
713 constant region locus involves highly homologous hot spots of recombination. *Genomics*
714 5: 431-441.
715 24. Bashirova, A. A., W. Zheng, M. Akdag, D. G. Augusto, N. Vince, K. L. Dong, C. O'HUigin,
716 and M. Carrington. 2021. Population-specific diversity of the immunoglobulin constant
717 heavy G chain (IGHG) genes. *Genes Immun* 22: 327-334.
718 25. Lefranc, M. P., G. Lefranc, G. de Lange, T. A. Out, P. J. van den Broek, J. van Nieuwkoop,
719 J. Radl, A. N. Helal, H. Chaabani, E. van Loghem, and et al. 1983. Instability of the human
720 immunoglobulin heavy chain constant region locus indicated by different inherited
721 chromosomal deletions. *Mol Biol Med* 1: 207-217.
722 26. Lefranc, M.-P., and G. Lefranc. 2012. Human Gm, Km, and Am Allotypes and Their
723 Molecular Characterization: A Remarkable Demonstration of Polymorphism. In
724 *Immunogenetics: Methods and Applications in Clinical Practice*. F. T. Christiansen, and B.
725 D. Tait, eds. Humana Press, Totowa, NJ. 635-680.
726 27. Lefranc, M.-P., G. Lefranc, and T. H. Rabbitts. 1982. Inherited deletion of immunoglobulin
727 heavy chain constant region genes in normal human individuals. *Nature* 300: 760-762.
728 28. van Erp, E. A., W. Luytjes, G. Ferwerda, and P. B. van Kasteren. 2019. Fc-Mediated
729 Antibody Effector Functions During Respiratory Syncytial Virus Infection and Disease.
730 *Front Immunol* 10.
731 29. Jefferis, R., J. Lund, and J. D. Pound. 1998. IgG-Fc-mediated effector functions: molecular
732 definition of interaction sites for effector ligands and the role of glycosylation.
733 *Immunological Reviews* 163: 59-76.

734 30. Vander Heiden, J. A., G. Yaari, M. Uduman, J. N. H. Stern, K. C. O'Connor, D. A. Hafler,
735 F. Vigneault, and S. H. Kleinstein. 2014. pRESTO: a toolkit for processing high-throughput
736 sequencing raw reads of lymphocyte receptor repertoires. *Bioinformatics* 30: 1930-1932.
737 31. Gupta, N. T., J. A. Vander Heiden, M. Uduman, D. Gadala-Maria, G. Yaari, and S. H.
738 Kleinstein. 2015. Change-O: a toolkit for analyzing large-scale B cell immunoglobulin
739 repertoire sequencing data. *Bioinformatics* 31: 3356-3358.
740 32. Charney, A. W., N. W. Simons, K. Mouskas, L. Lepow, E. Cheng, J. Le Berichel, C. Chang,
741 R. Marvin, D. M. Del Valle, S. Calorossi, A. Lansky, L. Walker, M. Patel, H. Xie, N. Yi, A.
742 Yu, G. Kang, A. Mendoza, L. E. Liharska, E. Moya, M. Hartnett, S. Hatem, L. Wilkins, M.
743 Eaton, H. Jamal, K. Tuballes, S. T. Chen, A. Tabachnikova, J. Chung, J. Harris, C.
744 Batchelor, J. Lacunza, M. Yishak, K. Argueta, N. Karekar, B. Lee, G. Kelly, D. Geanon, D.
745 Handler, J. Leech, H. Stefanos, T. Dawson, I. Scott, N. Francoeur, J. S. Johnson, A. Vaid,
746 B. S. Glicksberg, G. N. Nadkarni, E. E. Schadt, B. D. Gelb, A. Rahman, R. Sebra, G.
747 Martin, C. Agashe, P. Agrawal, A. Akyatan, K. Alesso-Carra, E. Alibo, K. Alvarez, A.
748 Amabile, S. Ascolillo, R. Bailey, P. Begani, P. B. Correra, S.-A. Brown, M. Buckup, L.
749 Burka, L. Cambron, G. Carrara, S. Chang, J. Chien, M. Chowdhury, C. C. Bozkus, P.
750 Comella, D. Cosgrove, F. Cossarini, L. Cotter, A. Dave, B. Dayal, M. Dhainaut, R.
751 Dornfeld, K. Dul, N. Eber, C. Elaiho, F. Fabris, J. Faith, D. Falci, S. Feng, B. Fennessy, M.
752 Fernandes, S. Gangadharan, J. Grabowska, G. Gyimesi, M. Hamdani, M. Herbinet, E.
753 Herrera, A. Hochman, G. E. Hoffman, J. Hook, L. Horta, E. Humblin, S. Karim, J. Kim, D.
754 Lebovitch, G. Lee, G. H. Lee, J. Lee, M. Leventhal, K. Lindblad, A. Livanos, R. Machado,
755 Z. Mahmood, K. Mar, S. Maskey, P. Matthews, K. Meckel, S. Mehandru, C. Mercedes, D.
756 Meyer, G. Mollaoglu, S. Morris, K. Nie, M. Nisenholtz, G. Ofori-Amanfo, K. Onel, M.
757 Ounadjela, V. Patel, C. Pruitt, S. Rathi, J. Redes, I. Reyes-Torres, A. Rodrigues, A.
758 Rodriguez, V. Roudko, E. Ruiz, P. Scalzo, P. Silva, A. S. Schanoski, M. Straw, S.
759 Tabachnikova, C. Teague, B. Upadhyaya, V. Van Der Heide, N. Vaninov, D. Wacker, H.

760 Walsh, C. M. Wilk, J. Wilson, K. M. Wilson, L. Xue, N.-a. Yeboah, S. Young, N. Zaks, R.
761 Zha, T. Marron, N. Beckmann, S. Kim-Schulze, S. Gnjatic, M. Merad, and C.-B. T. The
762 Mount Sinai. 2020. Sampling the host response to SARS-CoV-2 in hospitals under siege.
763 *Nature Medicine* 26: 1157-1158.
764 33. Woolley, C., J. Chariker, E. Rouchka, E. Ford, E. Hudson, S. Waigel, M. Smith, and T.
765 Mitchell. 2022. Reference long-read isoform-aware transcriptomes of four human
766 peripheral blood lymphocyte subsets *G3: Genes, Genomes, Genetics*
767 34. Nouri, N., and S. H. Kleinstein. 2018. A spectral clustering-based method for identifying
768 clones from high-throughput B cell repertoire sequencing data. *Bioinformatics* 34: i341-
769 i349.
770 35. Nouri, N., and S. H. Kleinstein. 2020. Somatic hypermutation analysis for improved
771 identification of B cell clonal families from next-generation sequencing data. *PLOS*
772 *Computational Biology* 16: e1007977.
773 36. Hoehn, K. B., O. G. Pybus, and S. H. Kleinstein. 2022. Phylogenetic analysis of migration,
774 differentiation, and class switching in B cells. *PLOS Computational Biology* 18: e1009885.
775 37. Rodriguez, O. L., W. S. Gibson, T. Parks, M. Emery, J. Powell, M. Strahl, G. Deikus, K.
776 Auckland, E. E. Eichler, W. A. Marasco, R. Sebra, A. J. Sharp, M. L. Smith, A. Bashir, and
777 C. T. Watson. 2020. A Novel Framework for Characterizing Genomic Haplotype Diversity
778 in the Human Immunoglobulin Heavy Chain Locus. *Front Immunol* 11.
779 38. Lefranc, M. P. 2001. IMGT, the international ImMunoGeneTics database. *Nucleic Acids*
780 *Res* 29: 207-209.
781 39. Li, H. 2018. Minimap2: pairwise alignment for nucleotide sequences. *Bioinformatics* 34:
782 3094-3100.
783 40. Li, H., B. Handsaker, A. Wysoker, T. Fennell, J. Ruan, N. Homer, G. Marth, G. Abecasis,
784 R. Durbin, and G. P. D. P. Subgroup. 2009. The Sequence Alignment/Map format and
785 SAMtools. *Bioinformatics* 25: 2078-2079.

786 41. Martin, M., M. Patterson, S. Garg, S. O Fischer, N. Pisanti, G. W. Klau, A. Schöenhuth,
787 and T. Marschall. 2016. WhatsHap: fast and accurate read-based phasing. *bioRxiv*:
788 085050.
789 42. Altschul, S. F., W. Gish, W. Miller, E. W. Myers, and D. J. Lipman. 1990. Basic local
790 alignment search tool. *J Mol Biol* 215: 403-410.
791 43. Fu, L., B. Niu, Z. Zhu, S. Wu, and W. Li. 2012. CD-HIT: accelerated for clustering the next-
792 generation sequencing data. *Bioinformatics (Oxford, England)* 28: 3150-3152.
793 44. Gadala-Maria, D., G. Yaari, M. Uduman, and S. H. Kleinstein. 2015. Automated analysis
794 of high-throughput B-cell sequencing data reveals a high frequency of novel
795 immunoglobulin V gene segment alleles. *Proceedings of the National Academy of*
796 *Sciences* 112: E862-E870.
797 45. Gadala-Maria, D., M. Gidoni, S. Marquez, J. A. Vander Heiden, J. T. Kos, C. T. Watson,
798 K. C. O'Connor, G. Yaari, and S. H. Kleinstein. 2019. Identification of Subject-Specific
799 Immunoglobulin Alleles From Expressed Repertoire Sequencing Data. *Front Immunol* 10.
800 46. Gidoni, M., O. Snir, A. Peres, P. Polak, I. Lindeman, I. Mikocziova, V. K. Sarna, K. E. A.
801 Lundin, C. Clouser, F. Vigneault, A. M. Collins, L. M. Sollid, and G. Yaari. 2019. Mosaic
802 deletion patterns of the human antibody heavy chain gene locus shown by Bayesian
803 haplotyping. *Nature Communications* 10: 628.
804 47. Peres, A., M. Gidoni, P. Polak, and G. Yaari. 2019. RAbHIT: R Antibody Haplotype
805 Inference Tool. *Bioinformatics* 35: 4840-4842.
806 48. Al'Khafaji, A. M., J. T. Smith, K. V. Garimella, M. Babadi, M. Sade-Feldman, M. Gatzen,
807 S. Sarkizova, M. A. Schwartz, V. Popic, E. M. Blaum, A. Day, M. Costello, T. Bowers, S.
808 Gabriel, E. Banks, A. A. Philippakis, G. M. Boland, P. C. Blainey, and N. Hacohen. 2021.
809 High-throughput RNA isoform sequencing using programmable cDNA concatenation.
810 *bioRxiv*: 2021.2010.2001.462818.

811 49. Brochu, H. N., E. Tseng, E. Smith, M. J. Thomas, A. M. Jones, K. R. Diveley, L. Law, S.
812 G. Hansen, L. J. Picker, M. Gale, and X. Peng. 2020. Systematic Profiling of Full-Length
813 Ig and TCR Repertoire Diversity in Rhesus Macaque through Long Read Transcriptome
814 Sequencing. *The Journal of Immunology* 204: 3434.
815 50. Kidd, M. J., Z. Chen, Y. Wang, K. J. Jackson, L. Zhang, S. D. Boyd, A. Z. Fire, M. M.
816 Tanaka, B. A. Gaëta, and A. M. Collins. 2012. The Inference of Phased Haplotypes for
817 the Immunoglobulin H Chain V Region Gene Loci by Analysis of VDJ Gene
818 Rearrangements. *The Journal of Immunology* 188: 1333.
819 51. Kirik, U., L. Greiff, F. Levander, and M. Ohlin. 2017. Parallel antibody germline gene and
820 haplotype analyses support the validity of immunoglobulin germline gene inference and
821 discovery. *Mol Immunol* 87: 12-22.
822 52. Irvine, E. B., and G. Alter. 2020. Understanding the role of antibody glycosylation through
823 the lens of severe viral and bacterial diseases. *Glycobiology* 30: 241-253.
824 53. Alter, G., T. H. M. Ottenhoff, and S. A. Joosten. 2018. Antibody glycosylation in
825 inflammation, disease and vaccination. *Seminars in Immunology* 39: 102-110.
826 54. Collin, M. 2020. Antibody glycosylation as an immunological key in health and disease.
827 *Glycobiology* 30: 200-201.
828 55. Plomp, R., L. R. Ruhaak, H.-W. Uh, K. R. Reiding, M. Selman, J. J. Houwing-Duistermaat,
829 P. E. Slagboom, M. Beekman, and M. Wuhrer. 2017. Subclass-specific IgG glycosylation
830 is associated with markers of inflammation and metabolic health. *Scientific Reports* 7:
831 12325.
832 56. Trampert, D. C., L. M. Hubers, S. F. J. van de Graaf, and U. Beuers. 2018. On the role of
833 IgG4 in inflammatory conditions: lessons for IgG4-related disease. *Biochimica et*
834 *Biophysica Acta (BBA) - Molecular Basis of Disease* 1864: 1401-1409.
835
836

837 **Figure Legends:**

838 **Figure 1. Overview of Ab structure and FLAIRR-seq molecular method.** (A) Schematic
839 representation of the IGH locus, heavy chain transcript structure, and functional IG protein. (B)
840 Comparative coverage across the heavy chain transcript of commonly used AIRR-seq methods
841 compared with FLAIRR-seq. (C) FLAIRR-seq molecular pipeline: RNA (brown) was converted to
842 first-strand cDNA (red) using the 5' RACE method, incorporating a 5' TSO-UMI (pink) via template
843 switch. Second strand amplification specifically targeted IgG and IgM molecules through priming
844 of the 5' TSO-UMI and the 3' constant region IGH exon 3 (CH3) for IgG, or CH4 for IgM. A 16bp
845 barcode was incorporated into the 3' CH3/CH4 primers to enable sample multiplexing post-
846 amplification. (D) IGV screenshot showing near full-length single molecule structure of IGHG4
847 FLAIRR-seq transcripts.

848 **Figure 2. FLAIRR-seq shows robust characterization of V, D, and J genes.** (A) Spearman
849 ranked correlations and p-values of V, D, and J gene usage frequencies identified by FLAIRR-
850 seq performed on matched total PBMC and purified B cells. (B) Heatmap of Spearman ranked
851 correlations and p-values of V, D and J gene usage frequencies between FLAIRR-seq and AIRR-
852 seq processed samples. (C) Boxplots of somatic hypermutation frequencies defined by FLAIRR-
853 seq or AIRR-seq in IgM- and IgG-specific repertoires. (D) Boxplots of CDR3 length defined by
854 FLAIRR-seq or AIRR-seq analysis in both IgM- and IgG-specific repertoires. (E) Spearman
855 ranked correlation of V, D, and J gene usage frequencies between FLAIRR-seq-based and Iso-
856 Seq-based repertoire profiling. Significant differences between FLAIRR-seq and AIRR-seq data
857 indicated by * ($p < 0.05$) or ** ($p < 0.01$).

858 **Figure 3. FLAIRR-seq provides novel IGHC resolution for allelic discovery and allows**
859 **variable gene haplotyping.** (A) Overview of experimental design and pipeline overviews of
860 genotyping by IGenotyper (gDNA) and FLAIRR-seq (RNA). (B) Schematic depicting IGHC alleles
861 identified by IGenotyper, partitioned by identification as (i) exact matches to documented IMGT

862 alleles, (ii) novel alleles that are not in IMGT, or (iii) extended alleles. (C) Pie chart and stacked
863 bar graph representing the total number of alleles and fraction of each category identified per
864 IGHC gene as identified by either IGenotyper or FLAIRR-seq. Bar charts showing number of
865 IGHC alleles from FLAIRR-seq that were resolved, ambiguous or unresolved when compared to
866 IGenotyper alleles. * Indicates additional allele found due to IGHG4 duplication. (D) Table
867 summarizing novel and extended alleles resolved by IGenotyper data. Extended alleles are
868 denoted by *(allele number)-FL and novel alleles are denoted by FL_(number) alleles resolved
869 by FLAIRR-seq are marked with a dot (•). (E) Venn diagrams showing number of IGHV haplotype
870 allele/deletion calls when using IGHJ6 or IGHM anchors for each haplotype. Tile plots showing
871 IGHV gene haplotypes inferred using either IGHJ6 anchors or IGHM anchors for one sample.
872 Dark gray represents a deletion (DEL), off-white a non-reliable allele annotation (NRA), and light
873 gray represents an unknown allele (Unk). Non-reliable alleles are annotated with an asterisk (*).

874 **Figure 4. FLAIRR-seq resolves subisotype specific repertoire diversity.** (A) Bar plots
875 showing distribution of unique VDJ sequences across isotypes, subisotypes, and subisotype
876 alleles in one representative sample, 1013, characterized by FLAIRR-seq. (B) Circos plots
877 showing V family gene usage frequency within each subisotype allele for sample 1013. (C)
878 Boxplots of V gene family usage frequencies within IGHG1, IGHG2, IGHG3, and IGHG4
879 repertoires across all ten individuals. (D) Principal component analysis of V gene family usage by
880 subisotype; plot includes the first two principal components, and individual repertoires are colored
881 by IGHG subisotype. (E) Boxplots showing sequence frequency of IGHV1 and IGHV3 family
882 genes by subisotype across all 10 samples.

883 **Figure 5. FLAIRR-seq resolves subisotype-specific clonal expansion and facilitates**
884 **haplotype analysis of CSR in a patient hospitalized for COVID-19.** (A) Overview of
885 experimental design: whole blood-derived RNA was collected on days 1, 4, 8 and 13 post-
886 hospitalization and used for FLAIRR-seq profiling. (B) Bar plot showing the percentage of clones

887 represented by each subisotype across timepoints. (C) Simpson's diversity index (q=2) for all
888 clones in each subisotype across four timepoints; IgG4 not included due to low sequence counts.
889 (D) Polarity, or the fraction of clones needed to comprise 80% of the repertoire, reported as
890 fraction of total subisotype-specific repertoires across time. (E) Distribution of a single clone
891 "9900" across isotypes and subisotypes over time, suggesting CSR of this clone. (F) Phylogenetic
892 tree constructed from sequences/members of clone 9900, with the inferred germline sequence
893 as the outgroup (star). Shapes and colors of tips (sequences) indicate time point and
894 isotype/subisotype. The scale bar represents the number of mutations between each node in the
895 tree. The subclade within the red box is represented by multiple time points and subisotypes,
896 providing evidence of CSR. (G) Tile plot showing the assignment of IGHC alleles to their
897 respective haplotypes, based on the frequency of observations in which each IGHC allele was
898 linked to each respective allele of heterozygous V genes, IGHV3-7 and IGHV3-48; light gray
899 denotes IGHC alleles for which haplotype assignment was not possible. Analysis of sequences
900 in (F) revealed that the IGHG1 and IGHG2 alleles represented in the phylogeny came from the
901 same haplotype (IGHG1*02/*07, IGHG2*08, IGHM_FL_2).
902

903

Table 1: Comparative analysis metrics between AIRR-seq and FLAIRR-seq on matched samples

Sample ID	Isotype	Method	RNA input (ng)	Input reads into Immcantation[a]	Post assembly /Single reads[b]	Unique VDJc	Unique Clones[d]	Unique CDR3[c]
0007	IgG	AIRR	100	**841627**	15217	3164	1008	1187
		FLAIRR	335	181109	17881	4880	1358	1520
201c	IgG	AIRR	100	**1509063**	25015	4568	1221	1371
		FLAIRR	296	221301	36053	10819	2145	2388
203c	IgG	AIRR	100	**1006965**	23085	5793	1436	1705
		FLAIRR	106	475703	14923	3778	993	1138
602c	IgG	AIRR	100	**1275902**	38078	7736	1542	2217
		FLAIRR	149	344906	33903	9225	1828	2357
705c	IgG	AIRR	100	**1113660**	15358	1362	557	576
		FLAIRR	268	279601	18627	2328	1063	1081
1008	IgG	AIRR	100	**1310350**	56848	12217	3005	3307
		FLAIRR	335	238820	57020	18235	3505	3813
1013	IgG	AIRR	100	**1158222**	25250	5027	1795	1964
		FLAIRR	222	396322	27871	7487	2565	2744
2008	IgG	AIRR	100	**835928**	21681	3900	1235	1368
		FLAIRR	240	418906	16441	4258	1308	1380
4002	IgG	AIRR	100	**632272**	8949	1112	727	772
		FLAIRR	335	398838	19692	5377	1719	1887
5001	IgG	AIRR	100	**695884**	13930	1885	1134	1244
		FLAIRR	335	313843	42845	12146	2226	2381
0007	IgM	AIRR	100	**841627**	12777	9154	7924	8163
		FLAIRR	335	331380	46384	14926	12367	12851
201c	IgM	AIRR	100	**1509063**	26850	17888	14281	14622
		FLAIRR	296	148355	98069	12803	9353	9573
203c	IgM	AIRR	100	**1006965**	24623	18189	16295	16629
		FLAIRR	106	509536	37527	10636	9315	9419
602c	IgM	AIRR	100	**1275902**	12306	8378	7704	7833
		FLAIRR	149	273103	48897	16406	14495	14745
705c	IgM	AIRR	100	**1113660**	19484	14273	12936	13413
		FLAIRR	268	435391	79251	17417	15706	16249
1008	IgM	AIRR	100	**1310350**	20264	12710	7878	8368
		FLAIRR	335	181063	47531	15284	8745	9276
1013	IgM	AIRR	100	**1158222**	12769	9012	8057	8241
		FLAIRR	222	262617	52508	17812	15291	15759
2008	IgM	AIRR	100	**835928**	11608	8551	5838	6206
		FLAIRR	240	502354	47596	14132	10225	10674
4002	IgM	AIRR	100	**632272**	18411	11607	11184	11367
		FLAIRR	335	489287	91732	22379	19000	21532
5001	IgM	FLAIRR	335	**313843**	10018	12146	2226	2381
		FLAIRR	355	171688	18944	6164	4866	5011

904

FIGURE 1.

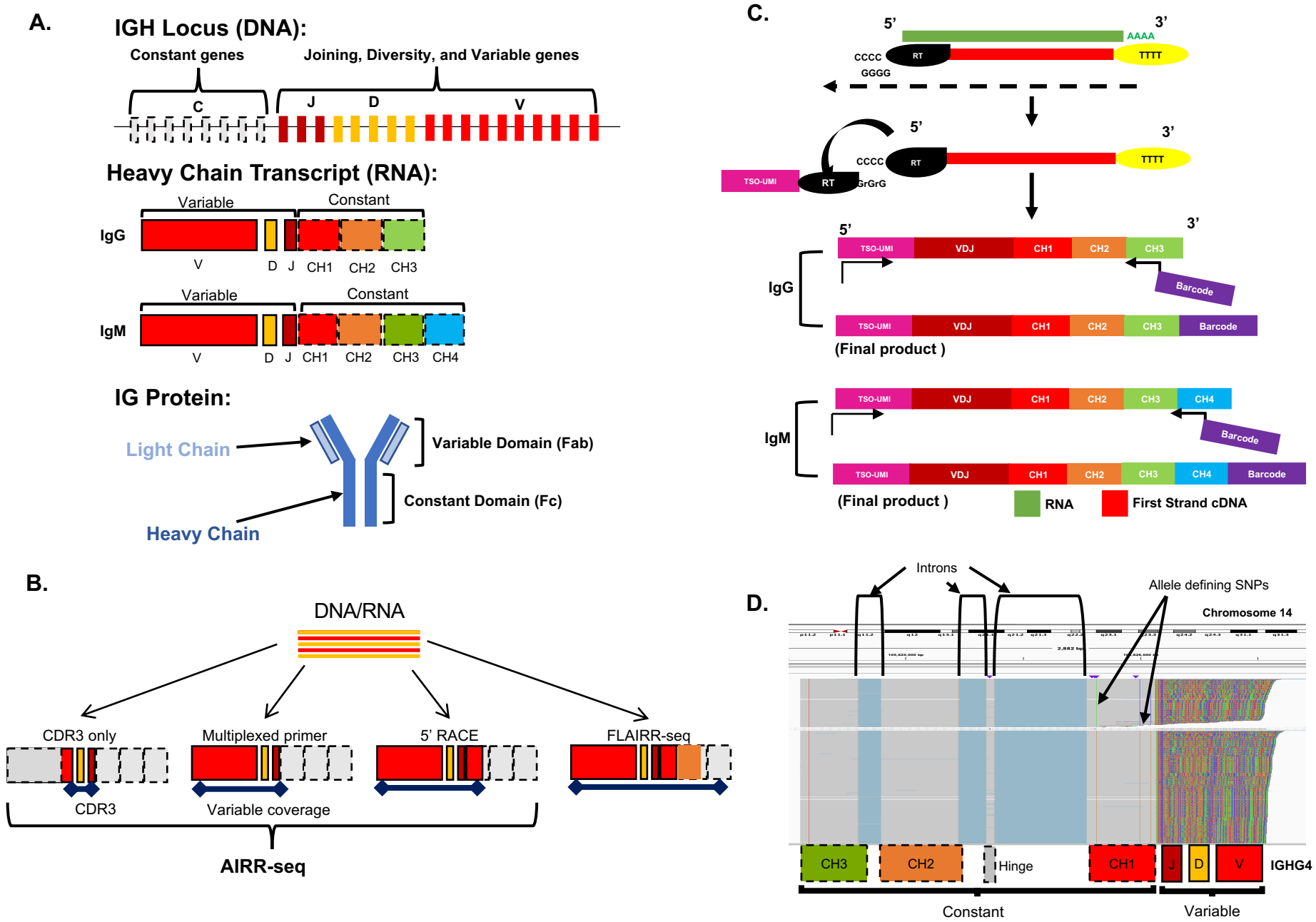
A.
IGH Locus (DNA):
Constant genes
Joining, Diversity, and Variable genes
C
J
D
V
Heavy Chain Transcript (RNA):
Variable
Constant
IgG
V
D
J
CH1
CH2
CH3
Variable
Constant
IgM
V
D
J
CH1
CH2
CH3
CH4
IG Protein:
Light Chain
Variable Domain (Fab)
Constant Domain (Fc)
Heavy Chain
B.
DNA/RNA
CDR3 only
Multiplexed primer
5' RACE
FLAIRR-seq
CDR3
Variable coverage
AIRR-seq
C.
5'
3'
AAAA
CCCC
GGGG
RT
TTTT
TSO-UMI
GrGrG
VDJ
CH1
CH2
CH3
CH4
Barcode
IgG
IgM
(Final product)
RNA
First Strand cDNA
D.
Introns
Allele defining SNPs
Chromosome 14
CH3
CH2
Hinge
CH1
J
D
V
IGHG4
Constant
Variable

FIGURE 2.

A. IgG BC vs. PBMC FLAIRR-seq

	V		D		J	
	r	p	r	p	r	p
1008	0.95	2.2e−16	0.95	2.2e−16	1.00	0.0028
0007	0.95	2.2e−16	0.95	4.1e−16	0.94	0.017
4002	0.95	2.2e−16	0.98	2.2e−16	0.89	0.033
705c	0.90	2.2e−16	0.97	2.2e−16	0.94	0.017

B. IgM

	V		D		J	
	r	p	r	p	r	p
0007	0.94	<2.2e-16	0.99	<2.2e-16	1.00	0.0028
201c	0.97	<2.2e-16	0.98	<2.2e-16	1.00	0.0028
203c	0.93	<2.2e-16	0.99	<2.2e-16	0.94	0.017
602c	0.96	<2.2e-16	0.99	<2.2e-16	1.00	0.0028
705c	0.95	<2.2e-16	0.99	<2.2e-16	0.94	0.017
1008	0.94	<2.2e-16	0.98	<2.2e-16	0.94	0.017
1013	0.96	<2.2e-16	0.99	<2.2e-16	0.94	0.017
2008	0.94	<2.2e-16	0.99	<2.2e-16	1.00	0.0028
4002	0.96	<2.2e-16	0.99	<2.2e-16	1.00	0.0028
5001	0.94	<2.2e-16	0.98	<2.2e-16	1.00	0.0028

IgG

	V		D		J	
	r	p	r	p	r	p
0007	0.93	<2.2e-16	0.94	1.6e-15	0.94	0.017
201c	0.96	<2.2e-16	0.96	<2.2e-16	0.89	0.033
203c	0.91	<2.2e-16	0.93	1.9e-14	0.94	0.017
602c	0.93	<2.2e-16	0.97	<2.2e-16	1.00	0.0028
705c	0.90	<2.2e-16	0.87	3.2e-10	1.00	0.0028
1008	0.95	<2.2e-16	0.99	<2.2e-16	1.00	0.0028
1013	0.95	<2.2e-16	0.95	<2.2e-16	0.89	0.033
2008	0.95	<2.2e-16	0.97	<2.2e-16	0.94	0.017
4002	0.95	<2.2e-16	0.93	6.1e-14	0.93	0.0077
5001	0.95	<2.2e-16	0.95	3.8e-16	1.00	0.0028

C.

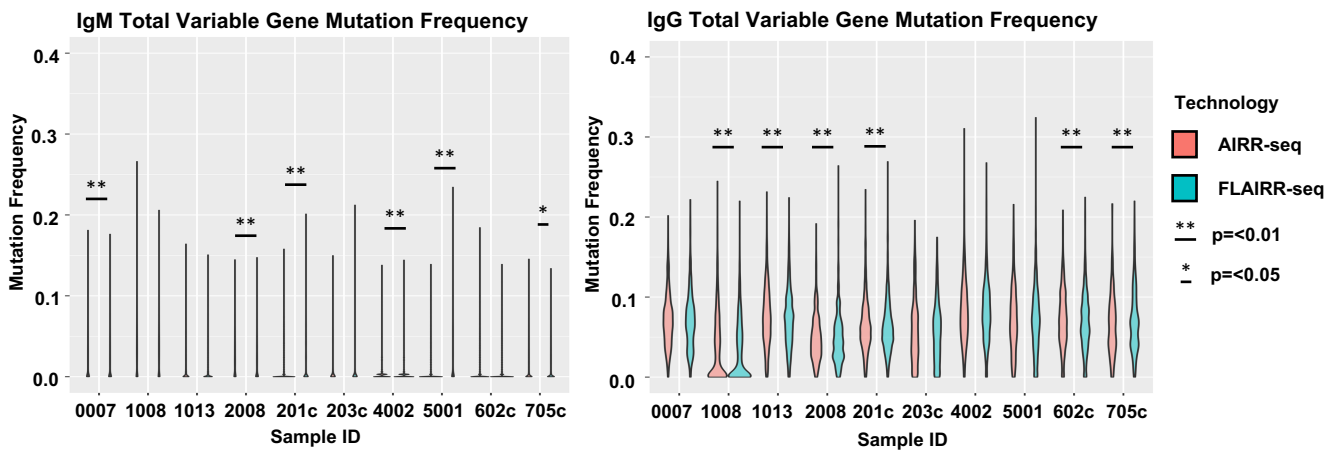

D.

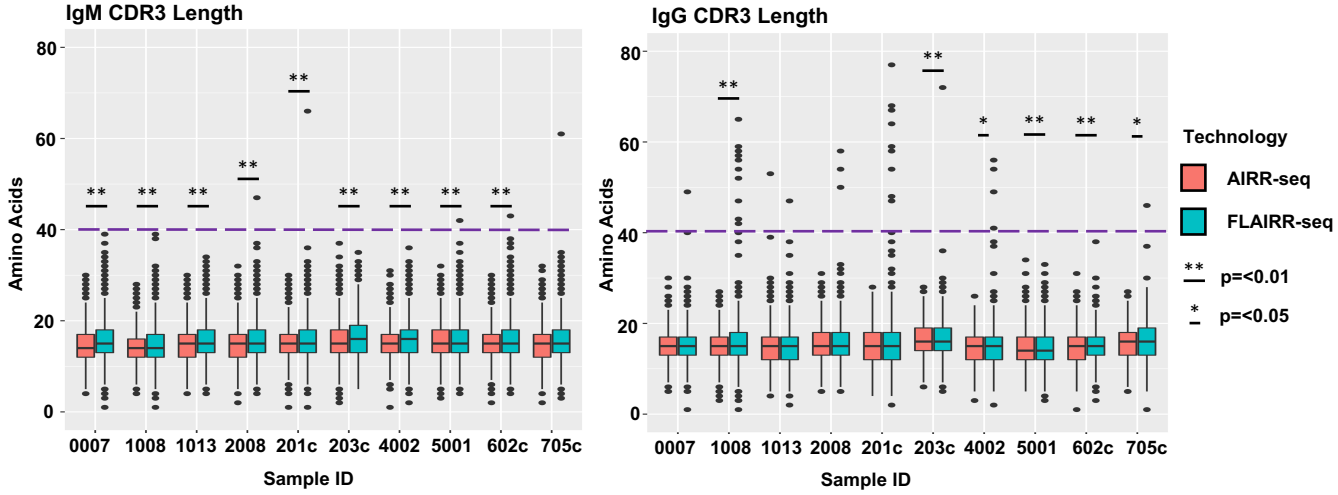

E. Iso-seq vs. FLAIRR-seq

	V		D		J	
	r	p	r	p	r	p
Sorted B cells	0.94	<2.2e-16	0.92	1.4e-13	1.00	0.0028

FIGURE 3.

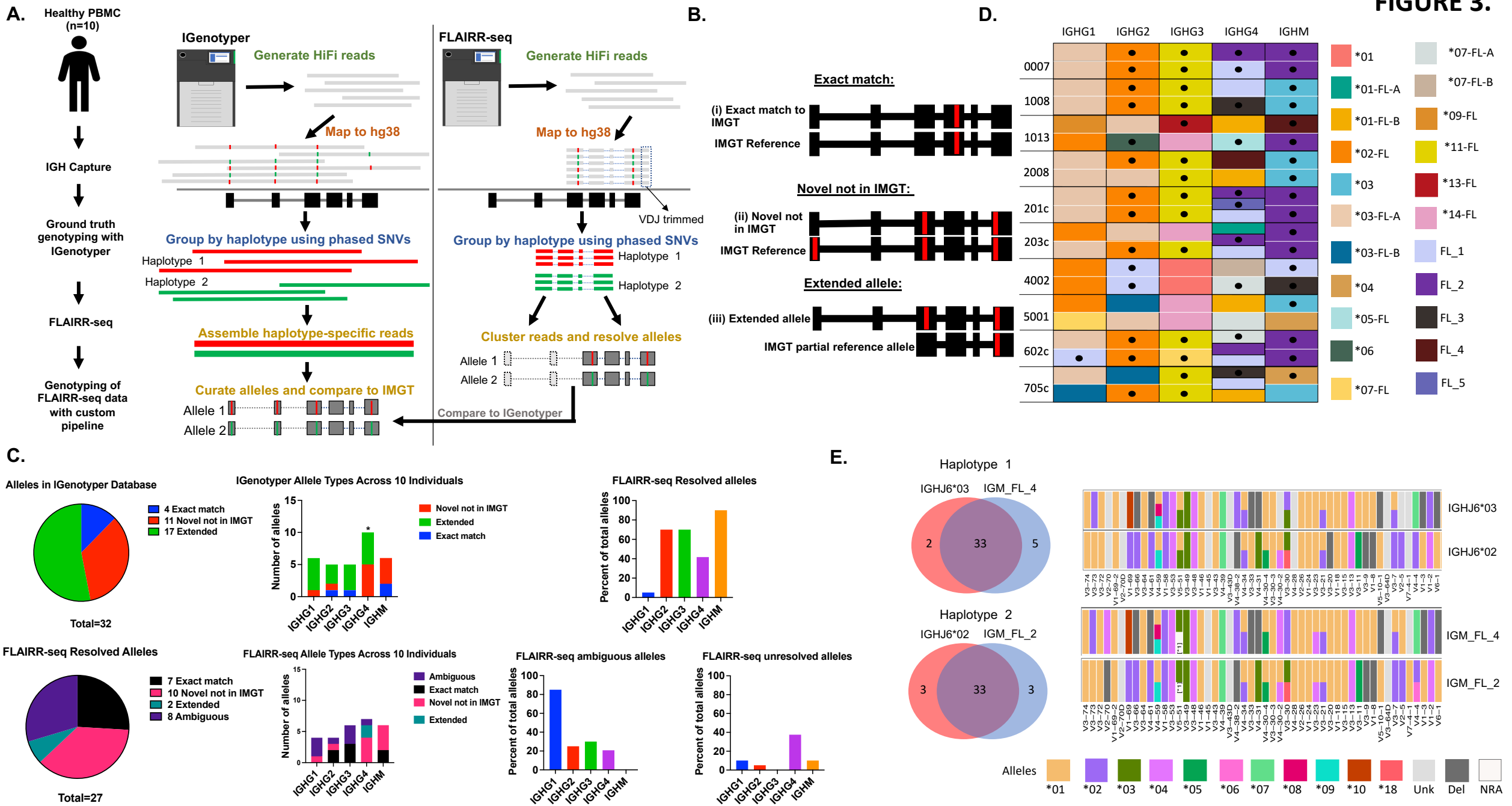
A.
Healthy PBMC (n=10)
IGH Capture
Ground truth genotyping with IGenotyper
FLAIRR-seq
Genotyping of FLAIRR-seq data with custom pipeline
IGenotyper
Generate HiFi reads
Map to hg38
Group by haplotype using phased SNVs
Haplotype 1
Haplotype 2
Assemble haplotype-specific reads
Curate alleles and compare to IMGT
Allele 1
Allele 2
FLAIRR-seq
Generate HiFi reads
Map to hg38
VDJ trimmed
Group by haplotype using phased SNVs
Haplotype 1
Haplotype 2
Cluster reads and resolve alleles
Allele 1
Allele 2
Compare to IGenotyper
B.
Exact match:
(i) Exact match to IMGT
IMGT Reference
Novel not in IMGT:
(ii) Novel not in IMGT
IMGT Reference
Extended allele:
(iii) Extended allele
IMGT partial reference allele
D.
IGHG1
IGHG2
IGHG3
IGHG4
IGHM
0007
1008
1013
2008
201c
203c
4002
5001
602c
705c
*01
*01-FL-A
*01-FL-B
*02-FL
*03
*03-FL-A
*03-FL-B
*04
*05-FL
*06
*07-FL
*07-FL-A
*07-FL-B
*09-FL
*11-FL
*13-FL
*14-FL
FL_1
FL_2
FL_3
FL_4
FL_5
C.
Alleles in IGenotyper Database
4 Exact match
11 Novel not in IMGT
17 Extended
Total=32
IGenotyper Allele Types Across 10 Individuals
Number of alleles
Novel not in IMGT
Extended
Exact match
IGHG1
IGHG2
IGHG3
IGHG4
IGHM
FLAIRR-seq Resolved alleles
Percent of total alleles
FLAIRR-seq Resolved Alleles
7 Exact match
10 Novel not in IMGT
2 Extended
8 Ambiguous
Total=27
FLAIRR-seq Allele Types Across 10 Individuals
Ambiguous
Exact match
Novel not in IMGT
Extended
FLAIRR-seq ambiguous alleles
FLAIRR-seq unresolved alleles
E.
Haplotype 1
IGHJ6*03
IGM_FL_4
2
33
5
Haplotype 2
IGHJ6*02
IGM_FL_2
3
33
3
IGHJ6*03
IGHJ6*02
IGM_FL_4
IGM_FL_2
Alleles
*01
*02
*03
*04
*05
*06
*07
*08
*09
*10
*18
Unk
Del
NRA

FIGURE 4.

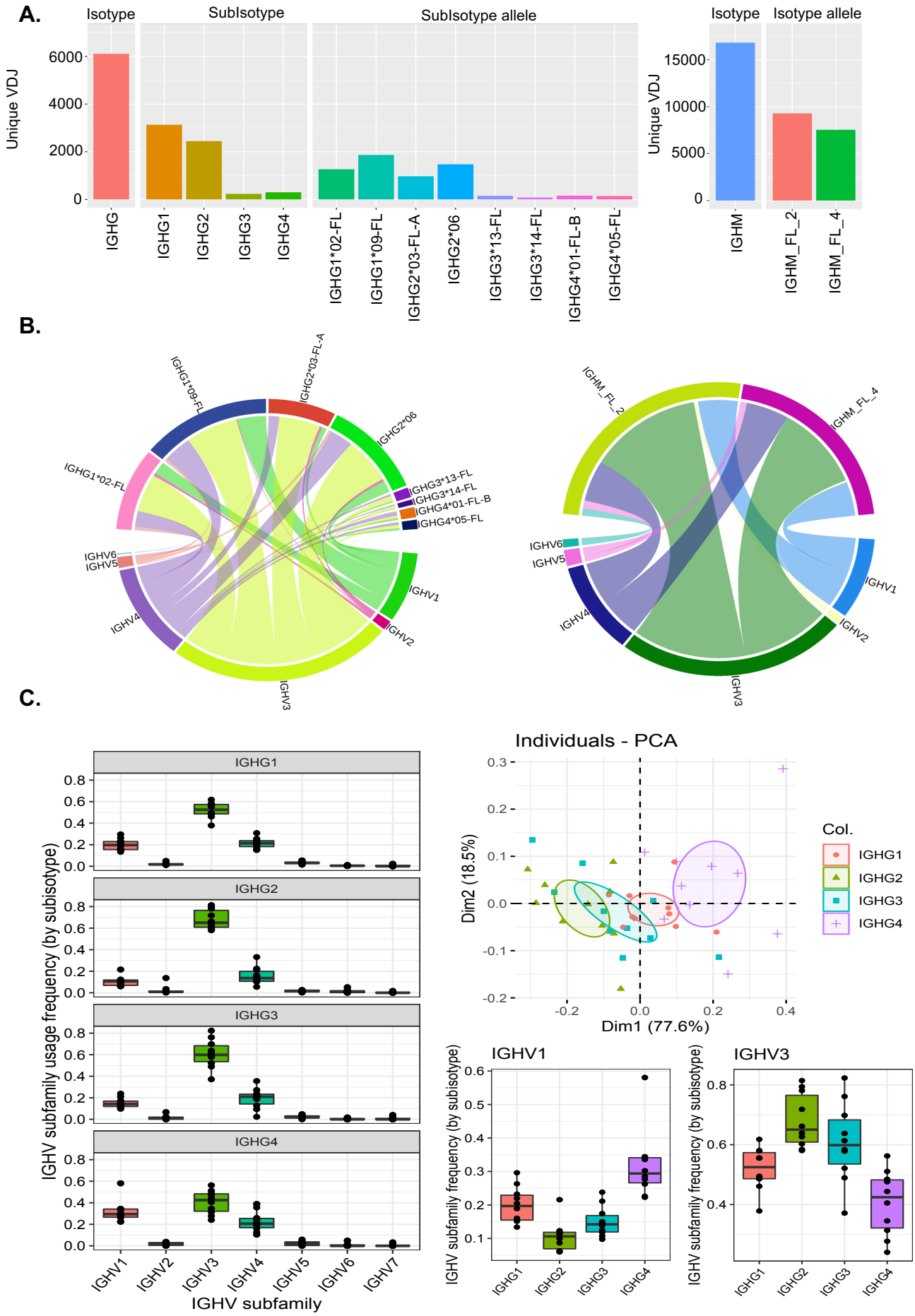
A.
Isotype
SubIsotype
SubIsotype allele
Isotype
Isotype allele
Unique VDJ
IGHG
IGHG1
IGHG2
IGHG3
IGHG4
IGHG1*02-FL
IGHG1*09-FL
IGHG2*03-FL-A
IGHG2*06
IGHG3*13-FL
IGHG3*14-FL
IGHG4*01-FL-B
IGHG4*05-FL
IGHM
IGHM_FL_2
IGHM_FL_4
B.
C.
IGHG1
IGHG2
IGHG3
IGHG4
IGHV subfamily usage frequency (by subisotype)
IGHV1
IGHV2
IGHV3
IGHV4
IGHV5
IGHV6
IGHV7
IGHV subfamily
Individuals - PCA
Dim1 (77.6%)
Dim2 (18.5%)
Col.
IGHV subfamily frequency (by subisotype)

FIGURE 5.

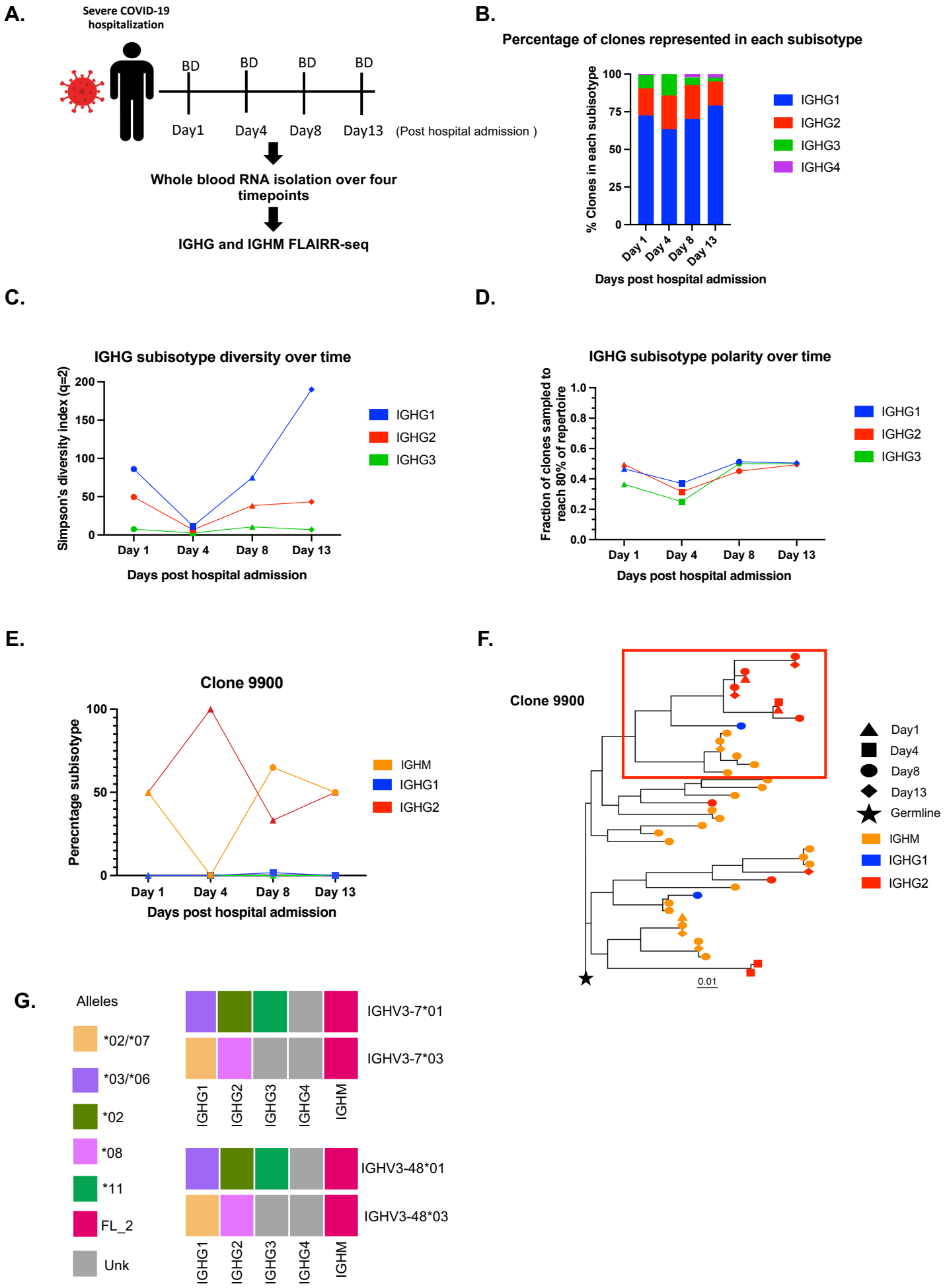
A.
Severe COVID-19 hospitalization
BD
BD
BD
BD
Day1
Day4
Day8
Day13
(Post hospital admission)
Whole blood RNA isolation over four timepoints
IGHG and IGHM FLAIRR-seq
B.
Percentage of clones represented in each subisotype
% Clones in each subisotype
100
75
50
25
0
Day 1
Day 4
Day 8
Day 13
Days post hospital admission
IGHG1
IGHG2
IGHG3
IGHG4
C.
IGHG subisotype diversity over time
Simpson's diversity index (q=2)
200
150
100
50
0
Day 1
Day 4
Day 8
Day 13
Days post hospital admission
IGHG1
IGHG2
IGHG3
D.
IGHG subisotype polarity over time
Fraction of clones sampled to reach 80% of repertoire
1.0
0.8
0.6
0.4
0.2
0.0
Day 1
Day 4
Day 8
Day 13
Days post hospital admission
IGHG1
IGHG2
IGHG3
E.
Clone 9900
Perecntage subisotype
100
50
0
Day 1
Day 4
Day 8
Day 13
Days post hospital admission
IGHM
IGHG1
IGHG2
F.
Clone 9900
0.01
Day1
Day4
Day8
Day13
Germline
IGHM
IGHG1
IGHG2
G.
Alleles
*02/*07
*03/*06
*02
*08
*11
FL_2
Unk
IGHV3-7*01
IGHV3-7*03
IGHV3-48*01
IGHV3-48*03
IGHG1
IGHG2
IGHG3
IGHG4
IGHM